arXiv:hep-ph/0412101v1 7 Dec 2004

SLAC–PUB–10871
November 2004

Light-Front QCD*

Stanley J. Brodsky
Stanford Linear Accelerator Center
Stanford University, Stanford, California 94309
E-mail: sjbth@slac.stanford.edu

Invited lectures and talk presented at the
58th Scottish University Summer School In Physics: A NATO Advanced Study
Institute and the European Union Hadronic Physics 13 Summer Institute
(SUSSP58)
St. Andrews, Scotland
30 August–1 September 2004

---

[*] Work supported by Department of Energy contract DE–AC02–76SF00515.

Abstract

In these lectures, I survey a number of applications of light-front methods to hadron and nuclear physics phenomenology and dynamics, including light-front statistical physics. Light-front Fock-state wavefunctions provide a frame-independent representation of hadrons in terms of their fundamental quark and gluon degrees of freedom. Nonperturbative methods for computing LFWFs in QCD are discussed, including string/gauge duality which predicts the power-law fall-off at high momentum transfer of light-front Fock-state hadronic wavefunctions with an arbitrary number of constituents and orbital angular momentum. The AdS/CFT correspondence has important implications for hadron phenomenology in the conformal limit, including an all-orders derivation of counting rules for exclusive processes. One can also compute the hadronic spectrum of near-conformal QCD assuming a truncated AdS/CFT space. Given the LFWFs, one can compute form factors, heavy hadron decay amplitudes, hadron distribution amplitudes, and the generalized parton distributions underlying deeply virtual Compton scattering. The quantum fluctuations represented by the light-front Fock expansion leads to novel QCD phenomena such as color transparency, intrinsic heavy quark distributions, diffractive dissociation, and hidden-color components of nuclear wavefunctions. A new test of hidden color in deuteron photodisintegration is proposed. The origin of leading-twist phenomena such as the diffractive component of deep inelastic scattering, single-spin asymmetries, nuclear shadowing and antishadowing is also discussed; these phenomena cannot be described by light-front wavefunctions of the target computed in isolation. Part of the anomalous NuTeV results for the weak mixing angle θ_W could be due to the non-universality of nuclear antishadowing for charged and neutral currents.

1 Introduction

In principle, quantum chromodynamics provides a fundamental description of hadronic and nuclear structure and dynamics in terms of their elementary quark and gluon degrees of freedom. The theory has extraordinary properties such as color confinement [1], asymptotic freedom [2, 3], a complex vacuum structure, and it predicts an array of new forms of hadronic matter such as gluonium and hybrid states [4]. The phase structure of QCD [5] implies the formation of a quark-gluon plasma in high energy heavy-ion collisions [6] as well insight into the evolution of the early universe [7]. Its non-Abelian Yang Mills gauge theory structure provides the foundation for the electroweak interactions and the eventual unification of the electrodynamic, weak, and hadronic forces at very short distances.

The asymptotic freedom property of QCD explains why the strong interactions become weak at short distances, thus allowing hard processes to be interpreted directly in terms of the perturbative interactions of quark and gluon quanta. This in turn leads to factorization theorems [8, 9] for both inclusive and exclusive processes [10] which separate the hard scattering subprocesses which control the reaction from the nonperturbative physics of the interacting hadrons.

QCD becomes scale free and conformally symmetric in the analytic limit of zero quark mass and zero β function. Conversely, one can start with the conformal prediction and systematically incorporate the non-zero β function contributions into the scale of the running coupling. This "conformal correspondence principle" determines the form of the expansion polynomials for distribution amplitudes and the behavior of nonperturbative wavefunctions which control hard exclusive processes at leading twist. The conformal template also can be used to derive commensurate scale relations which connect observables in QCD without scale or scheme ambiguity.

Recently, a remarkable duality has been established between supergravity string theory in 10 dimensions and conformal supersymmetric extensions of QCD [11, 12, 13, 14]. The AdS/CFT correspondence is now leading to a new understanding of QCD at strong coupling and the implications of its near-conformal structure. As I will discuss here, the AdS/CFT correspondence of large N_C supergravity theory in higher-dimensional anti-de Sitter space with supersymmetric QCD in 4-dimensional space-time has important implications for hadron phenomenology in the conformal limit, including the nonperturbative derivation of counting rules for exclusive processes and the behavior of structure functions at large x_{bj}. String/gauge duality also predicts the QCD power-law fall-off of light-front Fock-state hadronic wavefunctions with arbitrary orbital angular momentum at high momentum transfer.

The Lagrangian density of QCD [15] has a deceptively simple form:

$$\mathcal{L} = \overline{\psi}(i\gamma_\mu D^\mu - m)\psi - \frac{1}{4}G^2_{\mu\nu} \qquad (1)$$

where the covariant derivative is $iD_\mu = i\partial_\mu - gA_\mu$ and where the gluon field strength is $G_{\mu\nu} = \frac{i}{g}[D_\mu, D_\nu]$. The structure of the QCD Lagrangian is dictated by two principles:

(i) local $SU(N_C)$ color gauge invariance – the theory is invariant when a quark field is rotated in color space and transformed in phase by an arbitrary unitary matrix $\psi(x) \to U(x)\psi(x)$ locally at any point x^μ in space and time; and (ii) renormalizability, which requires the appearance of dimension-four interactions. In principle, the only parameters of QCD are the quark masses and the QCD coupling determined from a single observable at a single scale.

Solving QCD from first principles is extremely challenging because of the non-Abelian three-point and four-point gluonic couplings contained in its Lagrangian. The analytic problem of describing QCD bound states is compounded not only by the physics of confinement, but also by the fact that the wavefunction of a composite of relativistic constituents has to describe systems of an arbitrary number of quanta with arbitrary momenta and helicities. The conventional Fock state expansion based on equal-time quantization quickly becomes intractable because of the complexity of the vacuum in a relativistic quantum field theory. Furthermore, boosting such a wavefunction from the hadron's rest frame to a moving frame is as complex a problem as solving the bound state problem itself. The Bethe-Salpeter bound state formalism, although manifestly covariant, requires an infinite number of irreducible kernels to compute the matrix element of the electromagnetic current even in the limit where one constituent is heavy.

The description of relativistic composite systems using light-front quantization is in contrast remarkably simple. The Heisenberg problem for QCD can be written in the form

$$H_{LC}|H\rangle = M_H^2|H\rangle \ , \tag{2}$$

where $H_{LC} = P^+P^- - P_\perp^2$ is the mass operator. The operator $P^- = P^0 - P^3$ is the generator of translations in the light-front time $x^+ = x^0 + x^3$. Its form is predicted from the QCD Lagrangian. The quantities $P^+ = P^0 + P^3$ and $P_\perp$ play the role of the conserved three-momentum. The simplicity of the light-front Fock representation relative to that in equal-time quantization arises from the fact that the physical vacuum state has a much simpler structure on the light cone. Indeed, kinematical arguments suggest that the light-front Fock vacuum is the physical vacuum state. This means that all constituents in a physical eigenstate are directly related to that state, and not disconnected vacuum fluctuations. In the light-front formalism the parton model is literally true.

Formally, the light-front expansion is constructed by quantizing QCD at fixed light-front time [16] $\tau = t + z/c$ and forming the invariant light-front Hamiltonian: $H_{LF}^{QCD} = P^+P^- - \vec{P}_\perp^2$ where $P^\pm = P^0 \pm P^z$ [17]. The momentum generators P^+ and $\vec{P}_\perp$ are kinematical; *i.e.*, they are independent of the interactions. The generator $P^- = i\frac{d}{d\tau}$ generates light-front time translations, and the eigen-spectrum of the Lorentz scalar H_{LF}^{QCD} gives the mass spectrum of the color-singlet hadron states in QCD together with their respective light-front wavefunctions.

Each hadronic eigenstate $|H\rangle$ of the QCD light-front Hamiltonian can be expanded on the complete set of eigenstates $\{|n\rangle\}$ of the free Hamiltonian which have the same global quantum numbers: $|H\rangle = \sum \psi_n^H(x_i, k_\perp, \lambda_i)|n\rangle$. For example, the proton state satisfies: $H_{LF}^{QCD} \mid \psi_p\rangle = M_p^2 \mid \psi_p\rangle$. This equation can be written as a Heisenberg matrix eigenvalue problem by introducing a complete set of free Fock states. The Fock expansion begins with the color singlet state $|uud\rangle$ of free quarks, and continues with $|uudg\rangle$ and the other quark and gluon states that span the degrees of freedom of the proton in QCD. The Fock states $\{|n\rangle\}$ are built on the free vacuum by applying the free light-front creation operators. The summation is over all momenta $(x_i, k_{\perp i})$ and helicities λ_i satisfying momentum conservation $\sum_i^n x_i = 1$ and $\sum_i^n k_{\perp i} = 0$ and conservation of the projection J^3 of angular momentum.

The light-front wavefunctions $\psi_{n/H}(x_i, \vec{k}_{\perp i}, \lambda_i)$ of hadrons are the central elements of QCD phenomenology, encoding the bound state properties of hadrons in terms of their fundamental quark and gluon degrees of freedom at the amplitude level. It is the probability amplitude that a proton of momentum $P^+ = P^0 + P^3$ and transverse momentum $P_\perp$ consists of n quarks and gluons with helicities λ_i and physical momenta $p_i^+ = x_i P^+$ and $p_{\perp i} = x_i P_\perp + k_{\perp i}$. The wavefunctions $\{\psi_n^p(x_i, k_{\perp i}, \lambda_i)\}, n = 3, \ldots$ thus describe the proton in an arbitrary moving frame. The variables $(x_i, k_{\perp i})$ are internal relative momentum coordinates. The fractions $x_i = p_i^+/P^+ = (p_i^0 + p_i^3)/(P^0 + P^3)$, $0 < x_i < 1$, are the boost-invariant light-front momentum fractions; $y_i = \log x_i$ is the difference between the rapidity of the constituent i and the rapidity of the parent hadron. The appearance of relative coordinates is connected to the simplicity of performing Lorentz boosts in the light-front framework. This is another major advantage of the light-front representation.

For example, the eigensolution $\mid \psi_p\rangle$ of the QCD light-front Hamiltonian for the proton expanded on the color-singlet $B = 1$, $Q = 1$ eigenstates $\{\mid n\rangle\}$ of the free Hamiltonian $H_{LF}^{QCD}(g = 0)$. This defines the light-front Fock expansion:

$$\begin{aligned} \left|\psi_p(P^+, \vec{P}_\perp)\right\rangle &= \sum_n \prod_{i=1}^n \frac{\mathrm{d}x_i\, \mathrm{d}^2\vec{k}_{\perp i}}{\sqrt{x_i}\, 16\pi^3}\ 16\pi^3\ \delta\left(1 - \sum_{i=1}^n x_i\right)\ \delta^{(2)}\left(\sum_{i=1}^n \vec{k}_{\perp i}\right) \\ &\quad \times \psi_{n/H}(x_i, \vec{k}_{\perp i}, \lambda_i) \left| n;\, x_i P^+, x_i\vec{P}_\perp + \vec{k}_{\perp i}, \lambda_i\right\rangle . \end{aligned} \tag{3}$$

The light-front momentum fractions $x_i = k_i^+/P^+$ and $\vec{k}_{\perp i}$ represent the relative momentum coordinates of the QCD constituents. The physical transverse momenta are $\vec{p}_{\perp i} = x_i \vec{P}_\perp + \vec{k}_{\perp i}$. The λ_i label the light-front spin projections S^z of the quarks and gluons along the quantization direction z. Each Fock component has the invariant mass squared

$$\mathcal{M}_n^2 = (\sum_{i=1}^n k_i^\mu)^2 = \sum_{i=1}^n \frac{k_{\perp i}^2 + m_i^2}{x_i}. \tag{4}$$

The physical gluon polarization vectors $\epsilon^\mu(k,\ \lambda = \pm 1)$ are specified in light-cone gauge by the conditions $k \cdot \epsilon = 0,\ \eta \cdot \epsilon = \epsilon^+ = 0$. The gluonic quanta which appear in the Fock states thus have physical polarization $\lambda = \pm 1$ and positive metric. Since each Fock particle is on its mass shell in a Hamiltonian framework, $k^- = k^0 - k^z = \frac{k_\perp^2 + m^2}{k^+}$.

The dominant configurations in the wavefunction are generally those with minimum values of $\mathcal{M}^2$. Note that, except for the case where $m_i = 0$ and $k_{\perp i} = 0$, the limit $x_i \to 0$ is an ultraviolet limit, *i.e.*, it corresponds to particles moving with infinite momentum in the negative z direction: $k_i^z \to -k_i^0 \to -\infty$.

LFWFs have the remarkable property of being independent of the hadron's four-momentum. In contrast, in equal-time quantization, a Lorentz boost mixes dynamically with the interactions, so that computing a wavefunction in a new frame at fixed t requires solving a nonperturbative problem as complicated as the Hamiltonian eigenvalue problem itself. The LFWFs are properties of the hadron itself; they are thus universal and process independent.

The central tool which will be used in these lectures are the light-front Fock state wavefunctions which encode the bound-state properties of hadrons in terms of their quark and gluon degrees of freedom at the amplitude level. Given these frame-independent wavefunctions, one can compute a large array of hadronic processes ranging from the generalized parton distributions measured in deep inelastic scatterings, hard exclusive reactions, and the weak decays of hadrons. As I will review below, the quantum fluctuations contained in the LFWFs lead to the prediction of novel QCD phenomena such as color transparency, intrinsic charm, sea quark asymmetries, and hidden color in nuclear wavefunctions.

Given the light-front wavefunctions $\{\psi_n(x_i, k_{\perp_i}, \lambda_i)\}$ one can compute the electromagnetic and weak form factors from a simple overlap of light-front wavefunctions, summed over all Fock states [18, 19]. Form factors are generally constructed from hadronic matrix elements of the current $\langle p|j^\mu(0)|p+q\rangle$, where in the interaction picture we can identify the fully interacting Heisenberg current J^μ with the free current j_μ at the spacetime point $x^\mu = 0$. In the case of matrix elements of the current $j^+ = j^0 + j^3$, in a frame with $q^+ = 0$, only diagonal matrix elements in particle number $n' = n$ are needed. In contrast, in the equal-time theory one must also consider off-diagonal matrix elements and fluctuations due to particle creation and annihilation in the vacuum. In the nonrelativistic limit one can make contact with the usual formulae for form factors in Schrödinger many-body theory.

One of the important aspects of fundamental hadron structure is the presence of non-zero orbital angular momentum in the bound-state wave functions. The evidence for a "spin crisis" in the Ellis-Jaffe sum rule signals a significant orbital contribution in the proton wave function [20, 21]. The Pauli form factor of nucleons is computed from the overlap of LFWFs differing by one unit of orbital angular momentum $\Delta L_z = \pm 1$. Thus the fact that the anomalous moment of the proton is non-zero requires nonzero orbital angular momentum in the proton wavefunction [19]. In the light-front method, orbital angular momentum is treated explicitly; it includes the orbital contributions induced by relativistic effects, such as the spin-orbit effects normally associated with the conventional Dirac spinors. Angular momentum conservation for each Fock state implies

$$J^z = \sum_i^n S_i^z + \sum_i^{n-1} L_i^z \tag{5}$$

where L_i^z is one of the $n-1$ relative orbital angular momenta.

The quark and gluon probability distributions of a hadron are constructed from integrals over the absolute squares $|\psi_n|^2$, summed over n. In the far off-shell domain of large parton virtuality, one can use perturbative QCD or conformal arguments to derive the asymptotic fall-off of the Fock amplitudes, which then in turn leads to the QCD evolution equations for distribution amplitudes and structure functions. More generally, one can prove factorization theorems for exclusive and inclusive reactions which separate the hard and soft momentum transfer regimes, thus obtaining rigorous predictions for the leading power behavior contributions to large momentum transfer cross sections. One can also compute the far off-shell amplitudes within the light-front wavefunctions where heavy quark pairs appear in the Fock states. Such states persist over a time $\tau \simeq P^+/\mathcal{M}^2$ until they are materialized in the hadron collisions. As I shall discuss, this leads to a number of novel effects in the hadroproduction of heavy quark hadronic states.

2 Light-Front Statistical Physics

As shown by Raufeisen and myself [22], one can construct a "light-front density matrix" from the complete set of light-front wavefunctions which is a Lorentz scalar. This form can be used at finite temperature to give a boost invariant formulation of thermodynamics. At zero temperature the light-front density matrix is directly connected to the Green's function for quark propagation in the hadron as well as deeply virtual Compton scattering. One can also define a light-front partition function Z_{LF} as an outer product of light-front wavefunctions. The deeply virtual Compton amplitude and generalized parton distributions can then be computed as the trace $Tr[Z_{LF}\mathcal{O}]$, where $\mathcal{O}$ is the appropriate local operator [22]. This partition function formalism can be extended to multi-hadronic systems and systems in statistical equilibrium to provide a Lorentz-invariant description of relativistic thermodynamics [22].

3 AdS/CFT and Hadron Phenomenology

Maldacena [11] has shown that there is a remarkable correspondence between large N_C supergravity theory in a higher dimensional anti-de Sitter space and supersymmetric QCD in 4-dimensional space-time. String/gauge duality provides a framework for predicting QCD phenomena based on the conformal properties of the AdS/CFT correspondence. For example, Polchinski and Strassler [12] have shown that the power-law fall-off of hard exclusive hadron-hadron scattering amplitudes at large momentum transfer can be derived without the use of perturbation theory by using the scaling properties of the hadronic interpolating fields in the large-r region of AdS space. Thus one can use the Maldacena correspondence to compute the leading power-law falloff of exclusive processes such as high-energy fixed-angle scattering of gluonium-gluonium scattering in supersymmetric QCD. The resulting predictions for hadron physics effectively coincide [12, 13, 14] with QCD dimensional counting rules [23, 24, 25, 26]. Polchinski and Strassler [12] have also derived counting rules for deep inelastic structure functions at $x \to 1$ in agreement with perturbative QCD predictions [27] as well as Bloom-Gilman exclusive-inclusive duality. An interesting point is that the hard scattering amplitudes which are normally or order α_s^p in PQCD appear as order $\alpha_s^{p/2}$ in the supergravity predictions. This can be understood as an all-orders resummation of the effective potential [11, 28]. The near-conformal scaling properties of light-front wavefunctions thus lead to a number of important predictions for QCD which are normally discussed in the context of perturbation theory.

De Teramond and I [29] have shown how one can use the scaling properties of the hadronic interpolating operator in the extended AdS/CFT space-time theory to determine the form of QCD wavefunctions at large transverse momentum $k_\perp^2 \to \infty$ and at $x \to 1$ [29]. The angular momentum dependence of the light-front wavefunctions also follow from the conformal properties of the AdS/CFT correspondence. The scaling and conformal properties of the correspondence leads to a hard component of the light-front Fock state wavefunctions of the form:

$$\begin{aligned}\psi_{n/h}(x_i, \vec{k}_{\perp i}, \lambda_i, l_{zi}) \quad &\sim \quad \frac{(g_s\ N_C)^{\frac{1}{2}(n-1)}}{\sqrt{N_C}} \prod_{i=1}^{n-1} (k_{i\perp}^{\pm})^{|l_{zi}|} \\ &\times \left[\frac{\Lambda_o}{M^2 - \sum_i \frac{\vec{k}_{\perp i}^2 + m_i^2}{x_i} + \Lambda_o^2}\right]^{n+\sum_i |l_{zi}|-1} ,\end{aligned} \tag{6}$$

where g_s is the string scale and Λ_o represents the basic QCD mass scale. The scaling predictions agree with the perturbative QCD analysis given in the references [30], but the AdS/CFT analysis is performed at strong coupling without the use of perturbation theory. The form of these near-conformal wavefunctions can be used as an initial ansatz for a variational treatment of the light-front QCD Hamiltonian. The same ansatz leads to predictions for the hadron spectrum,which I will discuss in the conclusions.

4 Light-Front Wavefunctions and Hadron Phenomenology

Even though QCD was motivated by the successes of the parton model, QCD predicts many new features which go well beyond the simple three-quark description of the proton. Since the number of Fock components cannot be limited in relativity and quantum mechanics, the nonperturbative wavefunction of a proton contains gluons and sea quarks, including heavy quarks at any resolution scale. Thus there is no scale Q_0 in deep inelastic lepton-proton scattering where the proton can be approximated by its valence quarks. The nonperturbative Fock state wavefunctions contain intrinsic gluons, strange quarks, charm quarks, etc., at any scale. The internal QCD interactions lead to asymmetries such as $s(x) \neq \overline{s}(x)$, $\overline{u}(x) \neq \overline{d}(x)$ and intrinsic charm and bottom distributions at large x since this minimizes the invariant mass and off-shellness of the higher Fock state. As discussed above, the Fock state expansion for nuclei contains hidden color states which cannot be classified in terms of nucleonic degrees of freedom. However, some leading-twist phenomena such as the diffractive component of deep inelastic scattering, single-spin asymmetries, nuclear shadowing and antishadowing cannot be computed from the LFWFs of hadrons in isolation.

4.1 The Strange Quark Asymmetry

In the simplest treatment of deep inelastic scattering, nonvalence quarks are produced via gluon splitting and DGLAP evolution. However, in the full theory, heavy quarks are multiply connected to the valence quarks [31]. Although the strange and antistrange distributions in the nucleon are identical when they derive from gluon-splitting $g \to s\overline{s}$, this is not the case when the strange quarks are part of the intrinsic structure of the nucleon – the multiple interactions of the sea quarks produce an asymmetry of the strange and anti-strange distributions in the nucleon due to their different interactions with the other quark constituents. A QED analogy is the distribution of τ^+ and τ^- in a higher Fock state of muonium $\mu^+ e^-$. The τ^- is attracted to the higher momentum μ^+ thus asymmetrically distorting its momentum distribution. Similar effects will happen in QCD. If we use the diquark model $|\,p\rangle \sim \left|\,u_{3_c}(ud)_{\overline{3}_C}\right\rangle$, then the Q_{3_C} in the $\left|\,u(ud)Q\overline{Q}\right\rangle$ Fock state will be attracted to the heavy diquark and thus have higher rapidity than the $\overline{Q}$. An alternative model is the $|\,K\Lambda\rangle$ fluctuation model for the $|\,uuds\overline{s}\rangle$ Fock state of the proton [32]. The s quark tends to have higher x.

Empirical evidence also continues to accumulate that the strange-antistrange quark distributions are not symmetric in the proton [32, 33, 34]. The experimentally observed asymmetry appears to be small but positive: $\int dx x[s(x) - \overline{s}(x)] > 0$. The results of a recent CTEQ global data analysis [35] of neutrino-induced dimuon data are shown in Fig. 1. The fit is constrained so that the number of s and $\overline{s}$ quarks in the nucleon are equal. The shape of the strangeness asymmetry is consistent with the ΛK fluctuation model [32]. Kretzner [33] has noted that a significant part of the NuTeV anomaly could be due to this asymmetry, The $\overline{s}(x) - s(x)$ asymmetry can be studied in detail in $p\overline{p}$ collisions by searching for antisymmetric forward-backward strange quark distributions in the $\overline{p} - p$ CM frame.

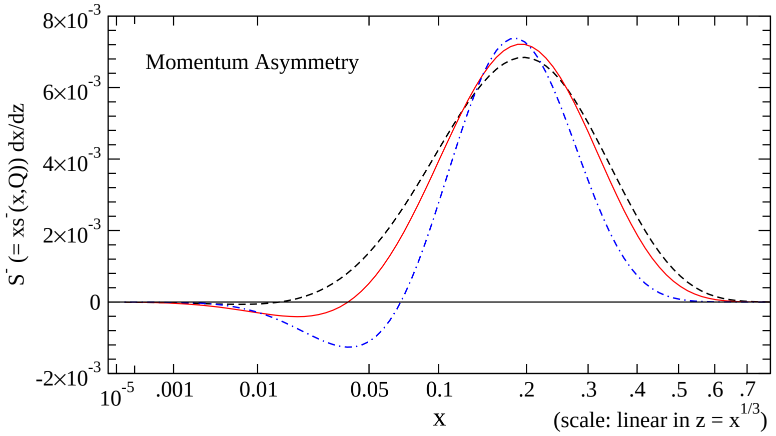

Figure 1: Representative results of the CTEQ strangeness asymmetry analysis.

4.2 Intrinsic Heavy Quarks

The probability for Fock states of a light hadron such as the proton to have an extra heavy quark pair decreases as $1/m_Q^2$ in non-Abelian gauge theory [36, 37]. The relevant matrix element is the cube of the QCD field strength $G^3_{\mu\nu}$. This is in contrast to abelian gauge theory where the relevant operator is $F^4_{\mu\nu}$ and the probability of intrinsic heavy leptons in QED bound state is suppressed as $1/m_\ell^4$. The intrinsic Fock state probability is maximized at minimal off-shellness. It is useful to define the transverse mass $m_{\perp i} = \sqrt{k^2_{\perp i} + m^2_i}$. The maximum probability then occurs at $x_i = m^i_\perp / \sum^n_{j=1} m^j_\perp$; *i.e.*, when the constituents have minimal invariant mass and equal rapidity. Thus the heaviest constituents have the highest momentum fractions and the highest x_i. Intrinsic charm thus predicts that the charm structure function has support at large x_{bj} in excess of DGLAP extrapolations [31]; this is in agreement with the EMC measurements [38].

Intrinsic charm can also explain the $J/\psi \to \rho\pi$ puzzle [39]. It also affects the extraction of suppressed CKM matrix elements in B decays [40].

4.3 Diffractive Dissociation and Intrinsic Heavy Quark Production

Diffractive dissociation is particularly relevant to the production of leading heavy quark states. The projectile proton can be decomposed as a sum over all of its Fock state components. The diffractive dissociation of the intrinsic charm $|uudc\bar{c}>$ Fock state of the proton on a nucleus can produce a leading heavy quarkonium state at high $x_F = x_c + x_{\bar{c}}$ in $pA \to J/\psi X A'$ since the c and $\bar{c}$ can readily coalesce into the charmonium state. Since the constituents of a given intrinsic heavy-quark Fock state tend to have the same rapidity, coalescence of multiple partons from the projectile Fock state into charmed hadrons and mesons is also favored. For example, as illustrated in Fig. 2, one can produce leading Λ_c at high x_F and low p_T from the coalescence of the udc constituents of the projectile IC Fock state. A similar coalescence mechanism was used in atomic physics to produce relativistic antihydrogen in $\overline{p}A$ collisions [41]. This phenomena is important not only for understanding heavy-hadron phenomenology, but also for understanding the sources of neutrinos in astrophysics experiments [42].

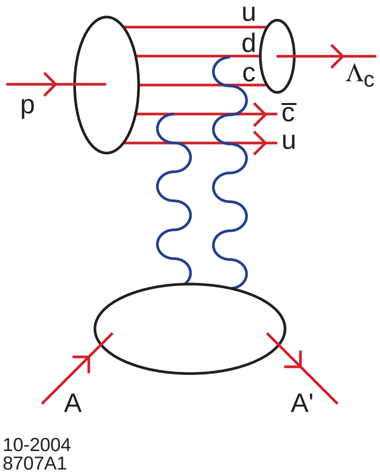

Figure 2: Production of forward heavy baryons by diffractive dissociation.

The charmonium state will be produced at small transverse momentum and high x_F with a characteristic $A^{2/3}$ nuclear dependence. This forward contribution is in addition to the A^1 contribution derived from the usual perturbative QCD fusion contribution at small x_F. Because of these two components, the cross section violates perturbative QCD factorization for hard inclusive reactions [43]. This is consistent with the observed two-component cross section for charmonium production observed by the NA3 collaboration at CERN [44].

The diffractive dissociation of the intrinsic charm Fock state leads to leading charm hadron production and fast charmonium production in agreement with measurements [45]. Intrinsic charm can also explain the $J/\psi \to \rho\pi$ puzzle [39], and it affects the extraction of suppressed CKM matrix elements in B decays [40]. Intrinsic charm can also enhance the production probability of Higgs bosons at hadron colliders from processes such as $gc \to Hc$. It is thus critical for new experiments (HERMES, HERA, COMPASS) to definitively establish the phenomenology of the charm structure function at large x_{bj}.

The production cross section for the double-charm Ξ_{cc}^+ baryon [46] and the production of J/ψ pairs appears to be consistent with the diffractive dissociation and coalescence of double IC Fock states [47, 48]. It is unlikely that the appearance of two heavy quarks at high x_F could be explained by the "color drag model" used in

PYTHIA simulations [49] in which the heavy quarks are accelerated from low to high x by the fast valence quarks. These observations provide compelling evidence for the diffractive dissociation of complex off-shell Fock states of the projectile and contradict the traditional view that sea quarks and gluons are always produced perturbatively via DGLAP evolution. It is also conceivable that the observations [50] of Λ_b at high x_F at the ISR in high energy pp collisions could be due to the diffractive dissociation and coalescence of the "intrinsic bottom" $|uudb\bar{b}>$ Fock states of the proton.

4.4 Color transparency

The small transverse size fluctuations of a hadron wavefunction with a small color dipole moment will have minimal interactions in a nucleus [51, 52].

This has been verified in the case of diffractive dissociation of a high energy pion into dijets $\pi A \to q\bar{q}A'$ in which the nucleus is left in its ground state [53]. As discussed in the next subsection, when the hadronic jets have balancing but high transverse momentum, one studies the small size fluctuation of the incident pion. The diffractive dissociation cross section is found to be proportional to A^2 in agreement with the color transparency prediction.

Color transparency has also been observed in diffractive electroproduction of ρ mesons [54] and in quasi-elastic $pA \to pp(A-1)$ scattering [55] where only the small size fluctuations of the hadron wavefunction enters the hard exclusive scattering amplitude. In the latter case an anomaly occurs at $\sqrt{s} \simeq 5$ GeV, most likely signaling a resonance effect at the charm threshold [56].

4.5 Diffraction Dissociation as a Tool to Resolve Hadron Substructure

Diffractive multi-jet production in heavy nuclei provides a novel way to measure the shape of light-front Fock state wave functions and test color transparency [52]. For example, consider the reaction [51, 57] $\pi A \to \mathrm{Jet}_1 + \mathrm{Jet}_2 + A'$ at high energy where the nucleus A' is left intact in its ground state. The transverse momenta of the jets balance so that $\vec{k}_{\perp i} + \vec{k}_{\perp 2} = \vec{q}_\perp < {R^{-1}}_A$. The light-front longitudinal momentum fractions also need to add to $x_1 + x_2 \sim 1$. Diffractive dissociation on a nucleus also requires that the energy of the beam has to be sufficiently large such that the momentum transfer to the nucleus $\Delta p_L = \frac{\Delta M^2}{2E_{lab}}$ is smaller than the inverse nuclear size R_A. The process can then occur coherently in the nucleus.

Because of color transparency, the valence wave function of the pion with small impact separation will penetrate the nucleus with minimal interactions, diffracting into jet pairs [51]. The $x_1 = x$, $x_2 = 1-x$ dependence of the di-jet distributions will thus reflect the shape of the pion valence light-front wave function in x; similarly, the $\vec{k}_{\perp 1} - \vec{k}_{\perp 2}$ relative transverse momenta of the jets gives key information on the second transverse momentum derivative of the underlying shape of the valence pion wavefunction [57, 58]. The diffractive nuclear amplitude extrapolated to $t = 0$ should be linear in nuclear number A if color transparency is correct. The integrated diffractive rate will then scale as $A^2/R_A^2 \sim A^{4/3}$. This is in fact what has been observed by the E791 collaboration at FermiLab for 500 GeV incident pions on nuclear targets [59]. The measured momentum fraction distribution of the jets is found to be approximately consistent with the shape of the pion asymptotic distribution amplitude, $\phi_\pi^{\rm asympt}(x) = \sqrt{3} f_\pi x(1-x)$ [60]. Data from CLEO [61] for the $\gamma\gamma^* \to \pi^0$ transition form factor also favor a form for the pion distribution amplitude close to the asymptotic solution to its perturbative QCD evolution equation [62, 63, 64].

Color transparency, as evidenced by the Fermilab measurements of diffractive dijet production, implies that a pion can interact coherently throughout a nucleus with minimal absorption, in dramatic contrast to traditional Glauber theory based on a fixed $\sigma_{\pi n}$ cross section. Color transparency gives direct validation of the gauge interactions of QCD.

4.6 Diffractive Dissociation and Hidden Color in Nuclear Wavefunctions

The concept of high energy diffractive dissociation can be generalized to provide a tool to materialize the individual Fock states of a hadron, nucleus or photon. For example, the diffractive dissociation of a high energy proton on a nucleus $pA \to XA'$ where the diffractive system is three jets $X = qqq$ can be used to determine the valence light-front wavefunction of the proton.

In the case of a deuteron projectile, one can study diffractive processes such as $dA \to pnA'$ or $dA \to \pi^- pp$ to measure the mesonic Fock state of a nuclear wavefunction. At small hadron transverse momentum, diffractive dissociation of the deuteron should be controlled by conventional nuclear interactions; however at large relative k_T, the diffractive system should be sensitive to the hidden color components of the deuteron wavefunction. The theory of hidden color is reviewed below.

5 DLCQ Solutions

The entire spectrum of hadrons and nuclei and their scattering states is given by the set of eigenstates of the light-front Hamiltonian H_{LC} for QCD. In principle it is possible to compute the light-front wavefunctions by diagonalizing the QCD light-front Hamiltonian on the free Hamiltonian basis. In the case of QCD in one space and one time dimensions, the application of discretized light-front quantization (DLCQ) [65] provides complete solutions of the theory, including the entire spectrum of mesons, baryons, and nuclei, and their wavefunctions. In the DLCQ method, one uses periodic boundary conditions in x^- and $b_\perp$ to discretize the light-front momentum space. One then diagonalizes the light-front Hamiltonian for QCD on a discretized Fock state basis. The DLCQ solutions can be obtained for arbitrary parameters including the number of flavors and colors and quark masses. Exact solutions are known for $QCD(1+1)$ at $N_C \to \infty$ by 't Hooft [66]. The one-space one-time theory can be solved numerically to any precision at finite N_C for any coupling strength and number of quark flavors using discretized light-front quantization (DLCQ) [65, 67, 68, 17]. One can use DLCQ to calculate the entire spectrum of virtually any 1+1 theory, its discrete bound states as well as the scattering continuum. The main emphasis of the DLCQ method applied to QCD is the determination of the wavefunctions of the hadrons from first principles.

A large number of studies have been performed of model field theories in the LF framework. This approach has been remarkably successful in a range of toy models in 1+1 dimensions: Yukawa theory [69], the Schwinger model (for both massless and massive fermions) [70, 71, 72], ϕ^4 theory [73, 74], QCD with various types of matter [75, 67, 76, 77], and the sine-Gordon model [78]. It has also been applied with promising results to theories in 3+1 dimensions, in particular QED [79, 80] and Yukawa theory [81] in a truncated basis. In all cases agreement was found between the LC calculations and results obtained by more conventional approaches, for example, lattice gauge theory.

The extension of this program to physical theories in 3+1 dimensions is a formidable computational task because of the much larger number of degrees of freedom; however, progress is being made. Analyses of the spectrum and light-front wavefunctions of positronium in QED_{3+1} are given in Ref. [79].

5.1 A DLCQ example: QCD_{1+1} with Fundamental Matter

This theory was originally considered by 't Hooft in the limit of large N_c [66]. Later Burkardt [75], and Hornbostel, *et al.* [67], gave essentially complete numerical solutions of the theory for finite N_c, obtaining the spectra of baryons, mesons, and nucleons and their wavefunctions. The DLCQ results are consistent with the few other calculations available for comparison, and are generally much more efficiently obtained. In particular, the mass of the lowest meson agrees to within numerical accuracy with lattice Hamiltonian results [82]. For $N_c = 4$ this mass is close to that obtained by 't Hooft in the $N_c \to \infty$ limit [66]. Finally, the ratio of baryon to meson mass as a function of N_c agrees with the strong-coupling results of Ref. [83].

In addition to the spectrum, one obtains the wavefunctions. These allow direct computation of, *e.g.*, structure functions. As an example, Fig. 3 shows the valence contribution to the structure function for an SU(3) baryon, for two values of the dimensionless coupling m/g. As expected, for weak coupling the distribution is peaked near $x = 1/3$, reflecting that the baryon momentum is shared essentially equally among its constituents. For comparison, the contributions from Fock states with one and two additional $q\bar{q}$ pairs are shown in Fig. 4. Note that the amplitudes for these higher Fock components are quite small relative to the valence configuration.

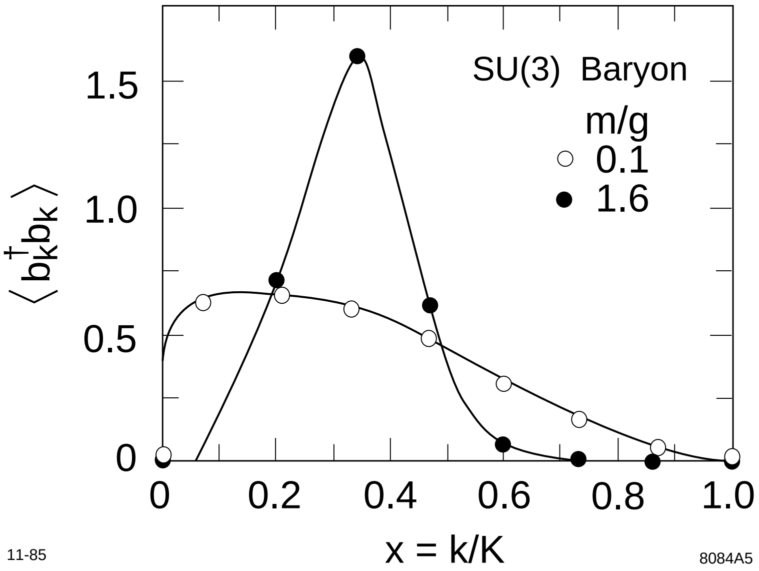

Figure 3: Valence contribution to the baryon structure function in QCD_{1+1}, as a function of the light-front longitudinal momentum fraction. The gauge group is SU(3), m is the quark mass, and g is the gauge coupling. (From Ref. [[67]].)

The lightest hadrons are nearly always dominated by the valence Fock state in these super-renormalizable models; higher Fock wavefunctions are typically suppressed by factors of 100 or more. Thus the light-front quarks are much more like constituent quarks in these theories than equal-time quarks would be. As discussed above, in an equal-time formulation even the vacuum state would be an infinite superposition of Fock states. Identifying constituents in this case, three of which could account for most of the structure of a baryon, would be quite difficult.

6 Light-Front Wavefunctions and Hadron Observables

Light-front Fock state wavefunctions $\psi_{n/H}(x_i, \vec{k}_{\perp i}, \lambda_i)$ play an essential role in QCD phenomenology, generalizing Schrödinger wavefunctions $\psi_H(\vec{k})$ of atomic physics to relativistic quantum field theory. Given the $\psi^{(\Lambda)}_{n/H}$, one can construct any spacelike electromagnetic, electroweak, or gravitational form factor or local operator product matrix element of a composite or elementary system from the diagonal overlap of the LFWFs [19]. Exclusive semi-leptonic B-decay amplitudes involving timelike currents such as $B \to A\ell\overline{\nu}$ can also be evaluated exactly in the light-front formalism [84]. In this case, the timelike decay matrix elements require the computation of both the diagonal matrix element $n \to n$ where parton number is conserved and the off-

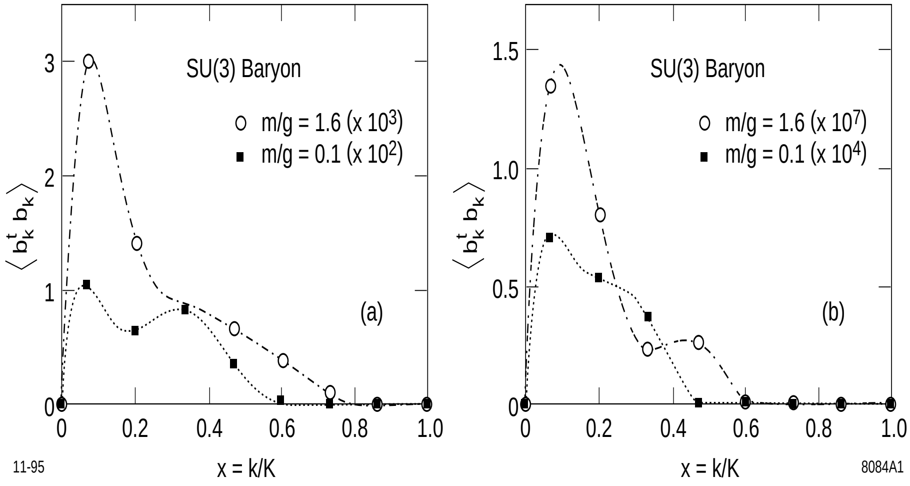

Figure 4: Contributions to the baryon structure function from higher Fock components: (a) valence plus one additional $q\overline{q}$ pair; (b) valence plus two additional $q\overline{q}$ pairs. (From Ref. [[67]].)

diagonal $n+1 \rightarrow n-1$ convolution such that the current operator annihilates a $q\overline{q'}$ pair in the initial B wavefunction. This term is a consequence of the fact that the time-like decay $q^2 = (p_\ell + p_{\overline{\nu}})^2 > 0$ requires a positive light-front momentum fraction $q^+ > 0$. Conversely for space-like currents, one can choose $q^+ = 0$, as in the Drell-Yan-West representation of the space-like electromagnetic form factors. The light-front Fock representation thus provides an exact formulation of current matrix elements of local operators. In contrast, in equal-time Hamiltonian theory, one must evaluate connected time-ordered diagrams where the gauge particle or graviton couples to particles associated with vacuum fluctuations. Thus even if one knows the equal-time wavefunction for the initial and final hadron, one cannot determine the current matrix elements. In the case of the covariant Bethe-Salpeter formalism, the evaluation of the matrix element of the current requires the calculation of an infinite number of irreducible diagram contributions.

One can also prove directly from the LFWF overlap representation that the anomalous gravitomagnetic moment $B(0)$ vanishes for any composite system [85]. This property follows directly from the Lorentz boost properties of the light-front Fock representation and holds separately for each Fock state component.

Given the light-front wave functions, one can define positive-definite probability distributions, such as the quark and gluon distributions $q(x, Q)$, $g(x, Q)$ which enter deep inelastic scattering and other hard inclusive reactions. This include all spin-dependent distributions such as quark transversity. The resulting distributions obey DGLAP evolution; the moments defined as the matrix elements of the operator product expansion have the correct anomalous dimensions. In addition one can compute the unintegrated distributions in x and $k_\perp$ which underlie the generalized parton distributions for nonzero skewness. example, the polarized quark distributions at resolution Λ correspond to

$$\begin{aligned} q_{\lambda_q/\Lambda_p}(x,\Lambda) &= \sum_{n,q_a} \int \prod_{j=1}^{n} dx_j d^2k_{\perp j} \sum_{\lambda_i} |\psi^{(\Lambda)}_{n/H}(x_i, \vec{k}_{\perp i}, \lambda_i)|^2 \\ &\times \delta\left(1 - \sum_i^n x_i\right) \delta^{(2)}\left(\sum_i^n \vec{k}_{\perp i}\right) \delta(x - x_q) \\ &\times \delta_{\lambda_a,\lambda_q} \Theta(\Lambda^2 - \mathcal{M}_n^2)\ , \end{aligned} \tag{7}$$

where the sum is over all quarks q_a which match the quantum numbers, light-front momentum fraction x, and helicity of the struck quark.

Diehl, Hwang, and I [86] have shown how to represent virtual Compton scattering $\gamma^* p \to \gamma p$ at large initial photon virtuality Q^2 and small momentum transfer squared t in handbag approximation in terms of the light-front wavefunctions of the target proton. Thus the generalized parton distributions which enter virtual Compton scattering and the two-photon exchange contribution to lepton-proton scattering are given by overlaps of the LFWFS with $n = n'$ and $n - n' = \pm 2$. One can verify that the skewed parton distributions $H(x, \zeta, t)$ and $E(x, \zeta, t)$ which appear in deeply virtual Compton scattering are the integrands of the Dirac and Pauli form factors $F_1(t)$ and $F_2(t)$ and the gravitational form factors $A_q(t)$ and $B_q(t)$ for each quark and anti-quark constituent. We have given an explicit illustration of the general formalism for the case of deeply virtual Compton scattering on the quantum fluctuations of a fermion in quantum electrodynamics at one loop. The absolute square of the LFWFS define the unintegrated parton distributions. The integrals of the unintegrated parton distributions over transverse momentum at zero skewness provide the helicity and transversity distributions measurable in polarized deep inelastic experiments [64].

The relationship of QCD processes to the hadron LFWFs is illustrated in Figs. 5 and 6. Other applications include two-photon exclusive reactions, and diffractive dissociation into jets. The universal light-front wave functions and distribution amplitudes control hard exclusive processes such as form factors, deeply virtual Compton scattering, high momentum transfer photoproduction, and two-photon processes.

Hadronization phenomena such as the coalescence mechanism for leading heavy hadron production can also be computed from LFWF overlaps. Diffractive jet production provides another phenomenological window into the structure of LFWFs. However, as shown recently [87] and discussed below, some leading-twist phenomena such as the diffractive component of deep inelastic scattering, single spin asymmetries, nuclear shadowing and antishadowing cannot be computed from the LFWFs of hadrons in isolation.

Given the LFWFs, one can also compute the hadronic distribution amplitudes $\phi_H(x_i, Q)$ which control hard exclusive processes as an integral over the transverse

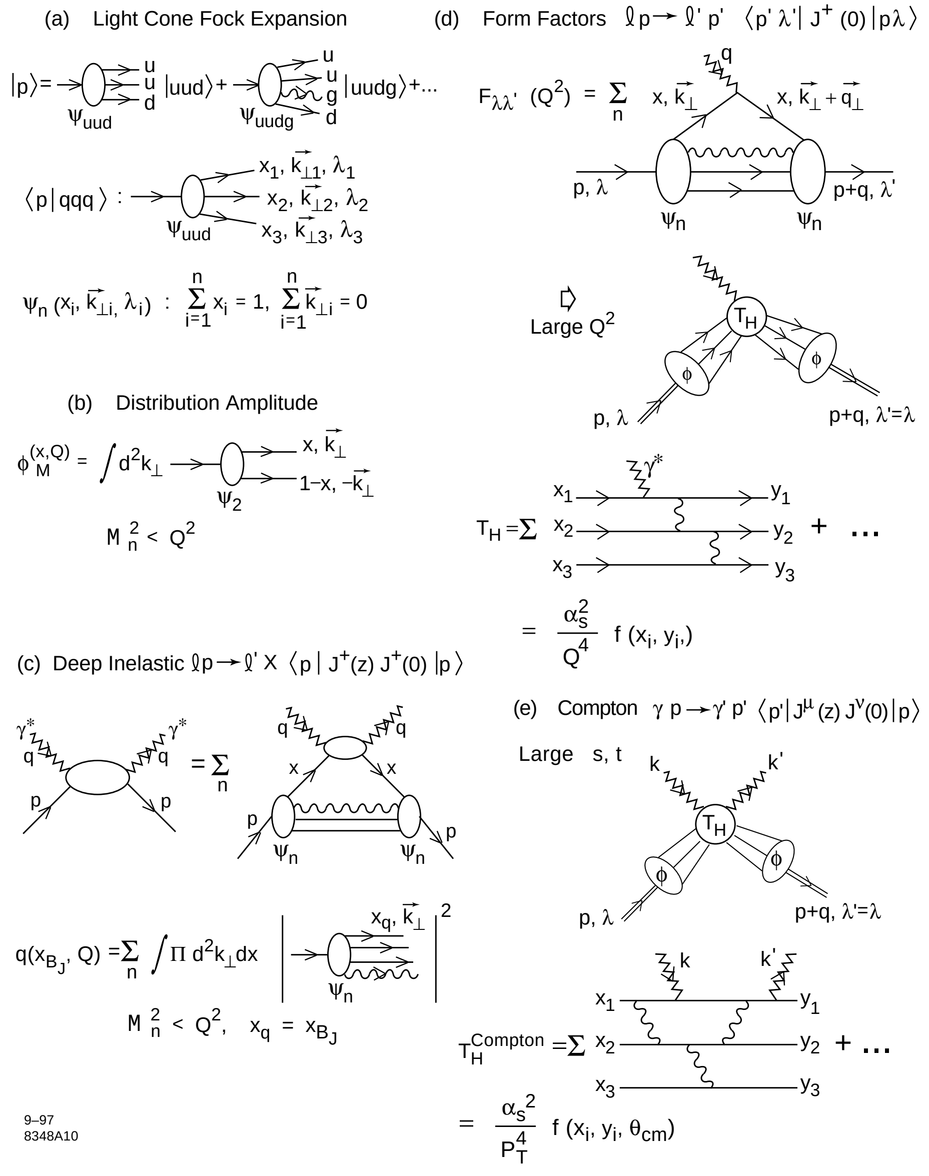
(a) Light Cone Fock Expansion
|p⟩= u u d |uud⟩+ u u g d |uudg⟩+...
Ψuud
Ψuudg
⟨p|qqq⟩ :
x1, k⊥1, λ1
x2, k⊥2, λ2
x3, k⊥3, λ3
Ψn (xi, k⊥i, λi) : Σ xi = 1, Σ k⊥i = 0
(b) Distribution Amplitude
φM(x,Q) = ∫d2k⊥
x, k⊥
1−x, −k⊥
Ψ2
M2n < Q2
(c) Deep Inelastic ℓp → ℓ' X ⟨p| J+(z) J+(0) |p⟩
γ*
q
p
= Σn
x
Ψn
q(xBJ, Q) = Σn ∫Π d2k⊥dx
xq, k⊥
M2n < Q2, xq = xBJ
9–97
8348A10
(d) Form Factors ℓp → ℓ' p' ⟨p' λ'| J+ (0) |pλ⟩
Fλλ' (Q2) = Σn
x, k⊥
x, k⊥ + q⊥
p, λ
p+q, λ'
Ψn
Large Q2
TH
φ
p+q, λ'=λ
γ*
x1
x2
x3
y1
y2
y3
TH = Σ
+ ...
= αs2/Q4 f (xi, yi,)
(e) Compton γ p → γ' p' ⟨p'|Jμ (z) Jν(0)|p⟩
Large s, t
k
k'
THCompton = Σ
= αs2/PT4 f (xi, yi, θcm)

Figure 5: Representation of QCD hadronic processes in the light-front Fock expansion. (a) The valence *uud* and higher Fock *uudg* contributions to the light-front Fock expansion for the proton. (b) The distribution amplitude $\phi(x,Q)$ of a meson expressed as an integral over its valence light-front wavefunction restricted to $q\overline{q}$ invariant mass less than Q. (c) Representation of deep inelastic scattering and the quark distributions $q(x,Q)$ as probabilistic measures of the light-front Fock wavefunctions. The sum is over the Fock states with invariant mass less than Q. (d) Exact representation of spacelike form factors of the proton in the light-front Fock basis. The sum is over all Fock components. At large momentum transfer the leading-twist contribution factorizes as the product of the hard scattering amplitude T_H for the scattering of the valence quarks collinear with the initial to final direction convoluted with the proton distribution amplitude. (e) Leading-twist factorization of the Compton amplitude at large momentum transfer.

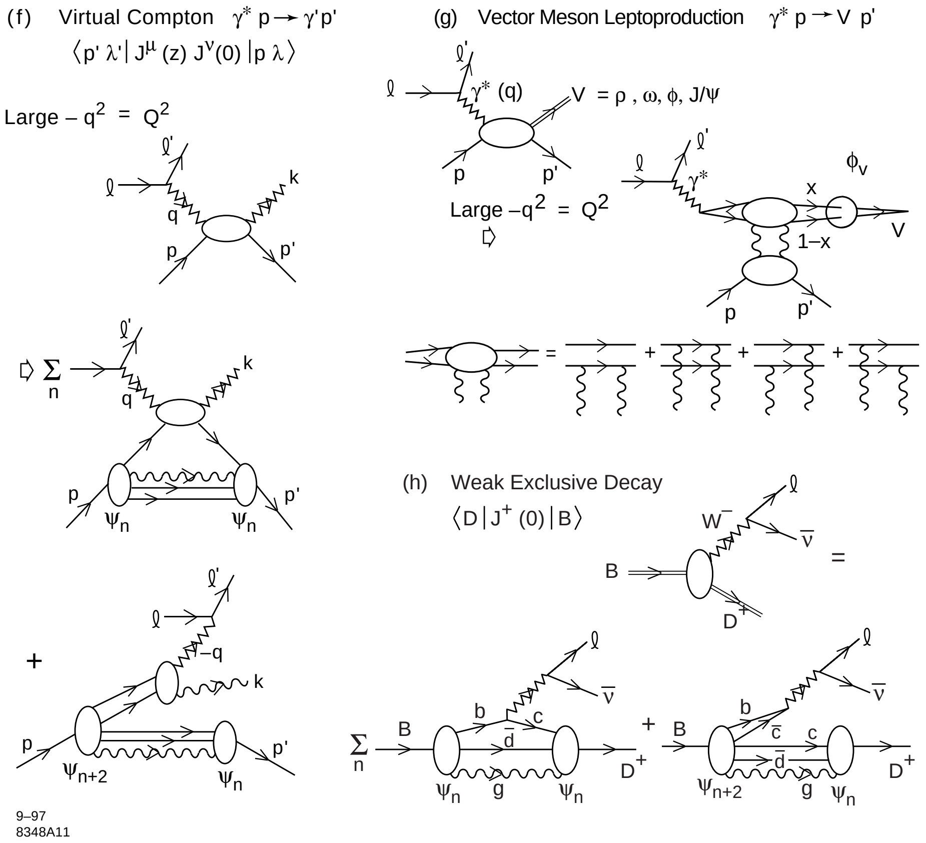

Figure 6: (f) Representation of deeply virtual Compton scattering in the light-front Fock expansion at leading twist. Both diagonal $n \to n$ and off-diagonal $n + 2 \to n$ contributions are required. (g) Diffractive vector meson production at large photon virtuality Q^2 and longitudinal polarization. The high energy behavior involves two gluons in the t channel coupling to the compact color dipole structure of the upper vertex. The bound-state structure of the vector meson enters through its distribution amplitude. (h) Exact representation of the weak semileptonic decays of heavy hadrons in the light-front Fock expansion. Both diagonal $n \to n$ and off-diagonal pair annihilation $n + 2 \to n$ contributions are required.

momenta of the valence Fock state LFWFs [64]. The hadron distribution amplitudes are obtained by integrating the $n-$parton valence light-front wavefunctions:

$$\phi(x_i, Q) = \int^Q \Pi_{i=1}^{n-1} d^2k_{\perp i} \; \psi_{\rm val}(x_i, k_\perp). \tag{8}$$

The distribution amplitudes are gauge-invariant vacuum to hadron matrix elements and they obey evolution equation as dictated by the OPE. Leading-twist PQCD predictions for hard exclusive amplitudes [64] are written in a factorized form as the product of hadron distribution amplitudes $\phi_I(x_i, Q)$ for each hadron I convoluted with the hard scattering amplitude T_H obtained by replacing each hadron with collinear on-shell quarks with light-front momentum fractions $x_i = k^+_i/P^+$. The logarithmic evolution equations for the distribution amplitudes require that the valence light-front wavefunctions fall-off asymptotically as the nominal power $[\frac{1}{k^2_\perp}]^{n-1}$, where n is the number of elementary fields in the minimal Fock state.

The light-front Fock representation thus provides an exact formulation of current matrix elements of local and bi-local operators. In contrast, in equal-time Hamiltonian theory, one must evaluate connected time-ordered diagrams where the gauge particle or graviton couples to particles associated with vacuum fluctuations. Thus even if one knows the equal-time wavefunction for the initial and final hadron, one cannot determine the current matrix elements. In the case of the covariant Bethe-Salpeter formalism, the evaluation of the matrix element of the current requires the calculation of an infinite number of irreducible diagram contributions.

7 General Structure of Light-Front Wavefunctions

Even without explicit solutions, much is known about the explicit form and structure of LFWFs. They can be matched to nonrelativistic Schrodinger wavefunctions at soft scales. At high momenta, the LFWFs at large $k_\perp$ and $x_i \to 1$ are constrained by arguments based on conformal symmetry, the operator product expansion, or perturbative QCD. The pattern of higher Fock states with extra gluons is given by ladder relations [88].

The structure of Fock states with nonzero orbital angular momentum is also constrained by the Karmanov-Smirnov operator [89]. One can define the light-front Fock expansion using a covariant generalization of light-front time: $\tau = x{\cdot}\omega$. The four-vector ω, with $\omega^2 = 0$, determines the orientation of the light-front plane; the freedom to choose ω provides an explicitly covariant formulation of light-front quantization [90]: all observables such as matrix elements of local current operators, form factors, and cross sections are light-front invariants – they must be independent of ω_μ. In recent work, Dae Sung Hwang, John Hiller, Volodya Karmonov and I [91] have studied the analytic structure of LFWFs using the explicitly Lorentz-invariant formulation of the front form. Eigensolutions of the Bethe-Salpeter equation have specific angular momentum as specified by the Pauli-Lubanski vector. The corresponding

LFWF for an n-particle Fock state evaluated at equal light-front time $\tau = \omega \cdot x$ can be obtained by integrating the Bethe-Salpeter solutions over the corresponding relative light-front energies. The resulting LFWFs $\psi^I_n(x_i, k_{\perp i})$ are functions of the light-front momentum fractions $x_i = k_i \cdot \omega / p \cdot \omega$ and the invariant mass of the constituents $\mathcal{M}_n$, each multiplying spin-vector and polarization tensor invariants which can involve ω^μ. They are eigenstates of the Karmanov–Smirnov kinematic angular momentum operator [89, 90].

$$\vec{J} = -i[\vec{k} \times \partial/\partial\vec{k}\,] - i[\vec{n} \times \partial/\partial\vec{n}] + \frac{1}{2}\vec{\sigma}, \tag{9}$$

where $\vec{n}$ is the spatial component of ω in the constituent rest frame ($\vec{\mathcal{P}} = \vec{0}$). Although this form is written specifically in the constituent rest frame, it can be generalized to an arbitrary frame by a Lorentz boost.

Normally the generators of angular rotations in the LF formalism contain interactions, as in the Pauli–Lubanski formulation; however, the LF angular momentum operator can also be represented in the kinematical form (9) without interactions. The key term is the generator of rotations of the LF plane $-i[\vec{n} \times \partial/\partial\vec{n}]$ which replaces the interaction term; it appears only in the explicitly covariant formulation, where the dependence on $\vec{n}$ is present. Thus LFWFs satisfy all Lorentz symmetries of the front form, including boost invariance, and they are proper eigenstates of angular momentum.

In principle, one can solve for the LFWFs directly from the fundamental theory using methods such as discretized light-front quantization (DLCQ) [69], the transverse lattice [92, 93, 94], lattice gauge theory moments [95], Dyson-Schwinger techniques [96], and Bethe–Salpeter techniques [91]. DLCQ has been remarkably successful in determining the entire spectrum and corresponding LFWFs in one space-one time field theories [97], including QCD(1+1) [67] and SQCD(1+1) [98]. There are also DLCQ solutions for low sectors of Yukawa theory in physical space-time dimensions [81]. The DLCQ boundary conditions allow a truncation of the Fock space to finite dimensions while retaining the kinematic boost and Lorentz invariance of light-front quantization.

One can also project known solutions of the Bethe–Salpeter equation to equal light-front time, thus producing hadronic light-front Fock wave functions [91]. Bakker and van Iersel have developed new methods to find solutions to bound-state light-front equations in ladder approximation [99]. Pauli has shown how one can construct an effective light-front Hamiltonian which acts within the valence Fock state sector alone [100]. Another possible method is to construct the $q\bar{q}$ Green's function using light-front Hamiltonian theory, DLCQ boundary conditions and Lippmann-Schwinger resummation. The zeros of the resulting resolvent projected on states of specific angular momentum J_z can then generate the meson spectrum and their light-front Fock wavefunctions. As emphasized by Weinstein and Vary, new effective operator methods [101, 102] which have been developed for Hamiltonian theories in condensed matter and nuclear physics, could also be applied advantageously to light-front Hamiltonian. Reviews of nonperturbative light-front methods may be found in references [17, 90, 103, 104].

Other important nonperturbative QCD methods are Dyson-Schwinger techniques [96] and the transverse lattice [93]. The transverse lattice method combines DLCQ for one-space and the light-front time dimensions with lattice theory in transverse space. It has recently provided the first computation of the generalized parton distributions of the pion [93].

Currently the most important computational tool for making predictions in strong-coupling QCD(3+1) is lattice gauge theory [105] which has made enormous progress in recent years, particularly in computing mass spectra and decay constants. Lattice gauge theory can only provide limited dynamical information because of the difficulty of continuing predictions from Euclidean to Minkowski space. At present, results are limited to large quark and pion masses such that the ρ meson is stable [106]. In contrast to lattice gauge theory path integral methods, Light-front Hamiltonian methods are frame-independent, formulated in Minkowski space, only two physical polarization gluonic degrees of freedom appear as quanta, and there is no complications from fermions. The known DLCQ solutions for 1+1 quantum field theories could provide a powerful test of lattice methods.

The Hamiltonian approach is in fact the method of choice in virtually every area of physics and quantum chemistry. It has the desirable feature that the output of such a calculation is immediately useful: the spectrum of states and wavefunctions. Furthermore, it allows the use of intuition developed in the study of simple quantum systems, and also the application of, *e.g.*, powerful variational techniques. The one area of physics where it is *not* widely employed is relativistic quantum field theory. The basic reason for this is that in a relativistic field theory quantized at equal time ("the Instant Form") one has particle creation/annihilation in the vacuum. Thus the true ground state is in general extremely complicated, involving a superposition of states with arbitrary numbers of bare quanta, and one must understand the complicated structure of this state before excitations can be considered. Furthermore, one must have a nonperturbative way of separating out disconnected contributions to physical quantities, which are physically irrelevant. Finally, the truncations that are required inevitably violate Lorentz covariance and, for gauge theories, gauge invariance. These difficulties (along with the development of covariant Lagrangian techniques) eventually led to the almost complete abandonment of fixed-time Hamiltonian methods in relativistic field theories.

Light-front quantization provides an alternative to the usual formulation of field theories in which these problems appear to be tractable. This raises the prospect of developing a practical Hamiltonian approach to solving field theories nonperturbatively based on diagonalizing LC Hamiltonians.

8 Consequences of Near-Conformal Field Theory

One of the most exciting recent developments is the AdS/CFT correspondence [11, 12, 13, 14] between superstring theory in 10 dimensions and supersymmetric Yang Mills theory in 3+1 dimensions. As I will discuss below, one can use this connection to establish the form of QCD wavefunctions at large transverse momentum $k_\perp^2 \to \infty$ and at $x \to 1$ [29]. The AdS/CFT correspondence has important implications for hadron phenomenology in the conformal limit, including an all-orders demonstration of counting rules [23, 24, 25] for hard exclusive processes [12], as well as determining essential aspects of hadronic light-front wavefunctions [29].

8.1 The Conformal Correspondence Principle

The classical Lagrangian of QCD for massless quarks is conformally symmetric. Since it has no intrinsic mass scale, the classical theory is invariant under the $SO(4,2)$ translations, boosts, and rotations of the Poincare group, plus the dilatations and other transformations of the conformal group. Scale invariance and therefore conformal symmetry is destroyed in the quantum theory by the renormalization procedure which introduces a renormalization scale as well as by quark masses. Conformal symmetry is thus broken in physical QCD; nevertheless, we can still recover the underlying features of the conformally invariant theory by evaluating any expression in QCD in the analytic limit of zero quark mass and zero β function [107]:

$$\lim_{m_q \to 0, \beta \to 0} \mathcal{O}_{QCD} = \mathcal{O}_{\text{conformal QCD}} \, . \tag{10}$$

This conformal correspondence limit is analogous to Bohr's correspondence principle where one recovers predictions of classical theory from quantum theory in the limit of zero Planck constant. The contributions to an expression in QCD from its nonzero β-function can be systematically identified [108, 109, 110] order-by-order in perturbation theory using the Banks-Zaks procedure [111].

The "conformal correspondence principle" provides a new tool, the conformal template [112, 113] , which is very useful for theory analyses, such as the expansion polynomials for distribution amplitudes [114, 115, 116, 117], the non-perturbative wavefunctions which control exclusive processes at leading twist [62, 118].

8.2 Commensurate Scale Relations

The near-conformal behavior of QCD is the basis for commensurate scale relations [119] which relate observables to each other without renormalization scale or scheme ambiguities [108, 109]. One can derive the commensurate scale relation between the effective charges of any two observables by first computing their relation in conformal gauge theory; the effects of the nonzero QCD $\beta-$ function are then taken into account using the BLM method [120] to set the scales of the respective couplings. An important example is the generalized Crewther relation [121]:

$$\left[1+\frac{\alpha_R(s^*)}{\pi}\right]\left[1-\frac{\alpha_{g_1}(Q^2)}{\pi}\right]=1 \tag{11}$$

where the underlying form at zero β function is dictated by conformal symmetry [122]. Here $\alpha_R(s)/\pi$ and $-\alpha_{g_1}(Q^2)/\pi$ represent the entire radiative corrections to $R_{e^+e^-}(s)$ and the Bjorken sum rule for the $g_1(x,Q^2)$ structure function measured in spin-dependent deep inelastic scattering, respectively. The relation between s^* and Q^2 can be computed order by order in perturbation theory using the BLM method [120]. The ratio of physical scales guarantees that the effect of new quark thresholds is commensurate. Commensurate scale relations are renormalization-scheme independent and satisfy the group properties of the renormalization group. Each observable can be computed in any convenient renormalization scheme such as dimensional regularization. The $\overline{MS}$ coupling can then be eliminated; it becomes only an intermediary [119]. In such a procedure there are no further renormalization scale (μ) or scheme ambiguities.

The effective charge [123] defined from the ratio of elastic pion and photon-to-pion transition form factors $\alpha_s^{\text{exclusive}}(Q^2)=F_\pi(Q^2)/4\pi Q^2F^2_{\gamma\pi^0}(Q^2)$ can also be connected to other effective charges and observables by commensurate scale relations. Its magnitude, $\alpha_s^{\text{exclusive}}(Q^2)\sim 0.8$ at small Q^2, is sufficiently large as to explain the observed magnitude of exclusive amplitudes such as the pion form factor using the asymptotic distribution amplitude. An analytic effective charge such as the pinch scheme [124] provides a method to unify the electroweak and strong couplings and forces.

8.3 Fixed Point Behavior

Although the QCD coupling decreases logarithmically at high virtuality due to asymptotic freedom, theoretical [125, 126, 127, 128, 129, 130, 131, 132] and phenomenological [133, 134, 135] evidence is now accumulating that the QCD coupling becomes constant at small virtuality; *i.e.*, $\alpha_s(Q^2)$ develops an infrared fixed point in contradiction to the usual assumption of singular growth in the infrared. If QCD running couplings are bounded, the integration over the running coupling is finite and renormalon resummations are not required. If the QCD coupling becomes scale-invariant in the infrared, then elements of conformal theory [117] become relevant even at relatively small momentum transfers.

Menke, Merino, and Rathsman and I have presented a definition of a physical coupling for QCD which has a direct relation to high precision measurements of the hadronic decay channels of the $\tau^-\to\nu_\tau\mathrm{H}^-$ [134] . Let R_τ be the ratio of the hadronic decay rate to the leptonic one. Then $R_\tau\equiv R^0_\tau\left[1+\frac{\alpha_\tau}{\pi}\right]$, where R^0_τ is the zeroth order QCD prediction, defines the effective charge α_τ. The data for τ decays is well-understood channel by channel, thus allowing the calculation of the hadronic decay rate and the effective charge as a function of the τ mass below the physical mass. The vector and axial-vector decay modes can be studied separately. Using an analysis of the τ data from the OPAL collaboration [132], we have found that the experimental value of the coupling $\alpha_\tau(s) = 0.621 \pm 0.008$ at $s = m_\tau^2$ corresponds to a value of $\alpha_{\overline{\rm MS}}(M_Z^2) = (0.117\text{-}0.122) \pm 0.002$, where the range corresponds to three different perturbative methods used in analyzing the data. This result is in good agreement with the world average $\alpha_{\overline{\rm MS}}(M_Z^2) = 0.117 \pm 0.002$. However, one also finds that the effective charge only reaches $\alpha_\tau(s) \sim 0.9 \pm 0.1$ at $s = 1\,\mathrm{GeV}^2$, and it even stays within the same range down to $s \sim 0.5\,\mathrm{GeV}^2$. The effective coupling is close to constant at low scales, suggesting that physical QCD couplings become constant or "frozen" at low scales.

Figure 7 shows a comparison of the experimentally determined effective charge $\alpha_\tau(s)$ with solutions to the evolution equation for α_τ at two-, three-, and four-loop order normalized at m_τ. At three loops the behavior of the perturbative solution drastically changes, and instead of diverging, it freezes to a value $\alpha_\tau \simeq 2$ in the infrared. The infrared behavior is not perturbatively stable since the evolution of the coupling is governed by the highest order term. This is illustrated by the widely different results obtained for three different values of the unknown four loop term $\beta_{\tau,3}$ which are also shown. The values of $\beta_{\tau,3}$ used are obtained from the estimate of the four loop term in the perturbative series of R_τ, $K_4^{\overline{\rm MS}} = 25 \pm 50$ [136]. It is interesting to note that the central four-loop solution is in good agreement with the data all the way down to $s \simeq 1\,\mathrm{GeV}^2$.

The results for α_τ resemble the behavior of the one-loop "time-like" effective coupling [137, 138, 139]

$$\alpha_{\rm eff}(s) = \frac{4\pi}{\beta_0}\left\{\frac{1}{2} - \frac{1}{\pi}\arctan\left[\frac{1}{\pi}\ln\frac{s}{\Lambda^2}\right]\right\} \tag{12}$$

which is finite in the infrared and freezes to the value $\alpha_{\rm eff}(s) = 4\pi/\beta_0$ as $s \to 0$. It is instructive to expand the "time-like" effective coupling for large s,

$$\begin{aligned}\alpha_{\rm eff}(s) &= \frac{4\pi}{\beta_0 \ln\left(s/\Lambda^2\right)}\left\{1 - \frac{1}{3}\frac{\pi^2}{\ln^2\left(s/\Lambda^2\right)} + \frac{1}{5}\frac{\pi^4}{\ln^4\left(s/\Lambda^2\right)} + \ldots\right\} \\ &= \alpha_{\rm s}(s)\left\{1 - \frac{\pi^2\beta_0^2}{3}\left(\frac{\alpha_{\rm s}(s)}{4\pi}\right)^2 + \frac{\pi^4\beta_0^4}{5}\left(\frac{\alpha_{\rm s}(s)}{4\pi}\right)^4 + \ldots\right\}.\end{aligned} \tag{13}$$

This shows that the "time-like" effective coupling is a resummation of $(\pi^2\beta_0^2\alpha_{\rm s}^2)^n$-corrections to the usual running couplings. The finite coupling $\alpha_{\rm eff}$ given in Eq. (12) obeys standard PQCD evolution at LO. Thus one can have a solution for the perturbative running of the QCD coupling which obeys asymptotic freedom but does not have a Landau singularity.

The near constancy of the effective QCD coupling at small scales helps explain the empirical success of dimensional counting rules for the power law fall-off of form

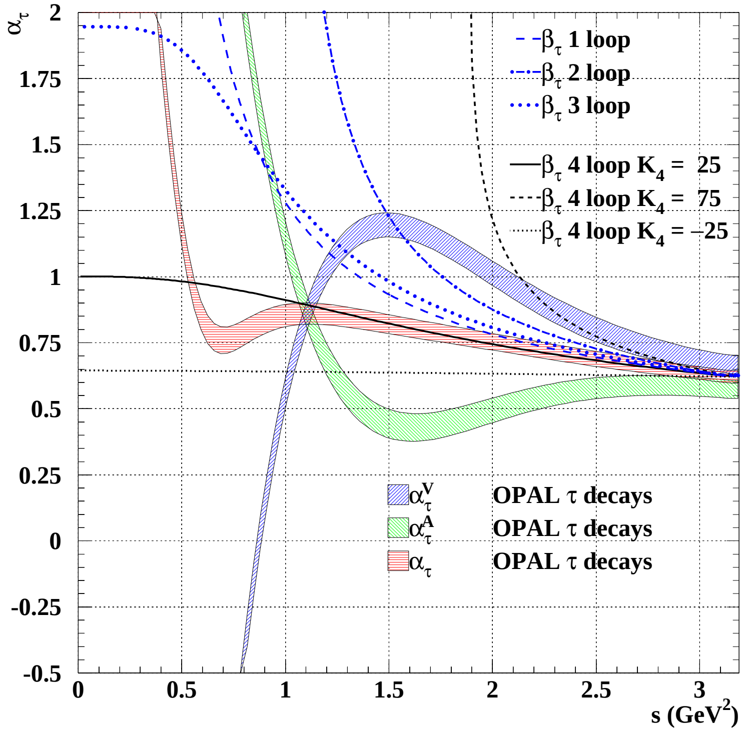

Figure 7: The effective charge α_τ for non-strange hadronic decays of a hypothetical τ lepton with $m^2_{\tau'} = s$ compared to solutions of the fixed order evolution equation for α_τ at two-, three-, and four-loop order. The error bands include statistical and systematic errors.

factors and fixed angle scaling. As shown in the references [123, 140], one can calculate the hard scattering amplitude T_H for such processes [64] without scale ambiguity in terms of the effective charge α_τ or α_R using commensurate scale relations. The effective coupling is evaluated in the regime where the coupling is approximately constant, in contrast to the rapidly varying behavior from powers of α_s predicted by perturbation theory (the universal two-loop coupling). For example, the nucleon form factors are proportional at leading order to two powers of α_s evaluated at low scales in addition to two powers of $1/q^2$; The pion photoproduction amplitude at fixed angles is proportional at leading order to three powers of the QCD coupling. The essential variation from leading-twist counting-rule behavior then only arises from the anomalous dimensions of the hadron distribution amplitudes.

8.4 The Abelian Correspondence Principle

Another important guide to QCD predictions is consistency in a limit where the theory becomes Abelian. One can consider QCD predictions as functions of analytic variables of the number of colors N_C and flavors N_F. At $N_C \to \infty$ at fixed $N_C \alpha_s$, calculations in QCD greatly simplify since only planar diagrams enter. However, the $N_C \to 0$ limit is also very interesting. Remarkably, one can show at all orders of perturbation theory [141] that PQCD predictions reduce to those of an Abelian theory similar to QED at $N_C \to 0$ with $C_F \alpha_s$ and $\frac{N_F}{T_F C_F}$ held fixed, where $C_F = \frac{N_C^2-1}{2N_C}$ and $T_F = 1/2$. The resulting theory corresponds to the group $1/U(1)$ which means that light-by-light diagrams acquire a particular topological factor. The $N_C \to 0$ limit provides an important check on QCD analyses; QCD formulae and phenomena must match their Abelian analog. The renormalization scale is effectively fixed by this requirement. Commensurate scale relations obey the Abelian Correspondence principle, giving the correct Abelian relations between observables in the limit $N_C \to 0$.

9 Perturbative QCD and Exclusive Processes

Exclusive processes constitute provide an important window on QCD processes and the structure of hadrons. There has been considerable progress analyzing exclusive and diffractive reactions at large momentum transfer from first principles in QCD. Rigorous statements can be made on the basis of asymptotic freedom and factorization theorems which separate the underlying hard quark and gluon subprocess amplitude from the nonperturbative physics of the hadronic wavefunctions. The leading-power contribution to exclusive hadronic amplitudes such as quarkonium decay, heavy hadron decay, and scattering amplitudes where hadrons are scattered with large momentum transfer can often be factorized as a convolution of distribution amplitudes $\phi_H(x_i, \Lambda)$ and hard-scattering quark/gluon scattering amplitudes T_H integrated over the light-front momentum fractions of the valence quarks [64]:

$$\mathcal{M}_{\rm Hadron} \;=\; \int \prod \phi_H^{(\Lambda)}(x_i, \lambda_i)\, T_H^{(\Lambda)} dx_i \ . \tag{14}$$

Here $T_H^{(\Lambda)}$ is the underlying quark-gluon subprocess scattering amplitude in which each incident and final hadron is replaced by valence quarks with collinear momenta $k_i^+ = x_i p_H^+$, $\vec{k}_{\perp i} = x_i \vec{p}_{\perp H}$. The invariant mass of all intermediate states in T_H is evaluated above the separation scale $\mathcal{M}_n^2 > \Lambda^2$. The essential part of the hadronic wavefunction is the distribution amplitude [64], defined as the integral over transverse momenta of the valence (lowest particle number) Fock wavefunction; *e.g.* for the pion

$$\phi_\pi(x_i, Q) \equiv \int d^2 k_\perp\, \psi^{(Q)}_{q\bar{q}/\pi}(x_i, \vec{k}_{\perp i}, \lambda) \tag{15}$$

where the separation scale Λ can be taken to be order of the characteristic momentum transfer Q in the process. It should be emphasized that the hard scattering amplitude

T_H is evaluated in the QCD perturbative domain where the propagator virtualities are above the separation scale.

The leading power fall-off of the hard scattering amplitude as given by dimensional counting rules follows from the nominal scaling of the hard-scattering amplitude: $T_H \sim 1/Q^{n-4}$, where n is the total number of fields (quarks, leptons, or gauge fields) participating in the hard scattering [25, 24]. Thus the reaction is dominated by subprocesses and Fock states involving the minimum number of interacting fields. In the case of $2 \to 2$ scattering processes, this implies

$$\frac{d\sigma}{dt}(AB \to CD) = F_{AB \to CD}(t/s)/s^{n-2} \tag{16}$$

where $n = N_A + N_B + N_C + N_D$ and n_H is the minimum number of constituents of H.

In the case of form factors, the dominant helicity conserving amplitude has the nominal power-law falloff $F_H(t) \sim (1/t)^{n_H - 1}$, The complete predictions from PQCD modify the nominal scaling by logarithms from the running coupling and the evolution of the distribution amplitudes. In some cases, such as large angle $pp \to pp$ scattering, there can be "pinch" contributions [142] when the scattering can occur from a sequence of independent near-on shell quark-quark scattering amplitudes at the same CM angle. After inclusion of Sudakov suppression form factors, these contributions also have a scaling behavior close to that predicted by constituent counting.

The constituent counting rules were originally derived in 1973 [25, 24] before the development of QCD in anticipation that the underlying theory of hadron physics would be renormalizable and close to a conformal theory. The factorized structure of hard exclusive amplitudes in terms of a convolution of valence hadron wavefunctions times a hard-scattering quark scattering amplitude was also proposed [25]. Upon the discovery of the asymptotic freedom in QCD, there was a systematical development of the theory of hard exclusive reactions, including factorization theorems, counting rules, and evolution equations for the hadronic distribution amplitudes [143, 144, 62, 145].

The distribution amplitudes which control leading-twist exclusive amplitudes at high momentum transfer can be related to the gauge-invariant Bethe-Salpeter wavefunction at equal light-front time $\tau = x^+$. The logarithmic evolution of the hadron distribution amplitudes $\phi_H(x_i, Q)$ with respect to the resolution scale Q can be derived from the perturbatively-computable tail of the valence light-front wavefunction in the high transverse momentum regime. The DGLAP evolution of quark and gluon distributions can also be derived in an analogous way by computing the variation of the Fock expansion with respect to the separation scale. Other key features of the perturbative QCD analyses are: (a) evolution equations for distribution amplitudes which incorporate the operator product expansion, renormalization group invariance, and conformal symmetry [64, 114, 146, 147, 148]; (b) hadron helicity conservation which follows from the underlying chiral structure of QCD [149]; (c) color transparency, which eliminates corrections to hard exclusive amplitudes from initial and final state interactions at leading power and reflects the underlying gauge theoretic basis for the strong interactions [52] and (d) hidden color degrees of freedom in nuclear wavefunctions, which reflect the color structure of hadron and nuclear wavefunctions [150]. There have also been recent advances eliminating renormalization scale ambiguities in hard-scattering amplitudes via commensurate scale relations [119] which connect the couplings entering exclusive amplitudes to the α_V coupling which controls the QCD heavy quark potential.

Exclusive processes such as $\overline{p}p \to \overline{p}p$, $\overline{p}p \to K^+K^-$ and $\overline{p}p \to \gamma\gamma$ provide a unique window for viewing QCD processes and hadron dynamics at the amplitude level [151, 118]. New tests of theory and comprehensive measurements of hard exclusive amplitudes can also be carried out for electroproduction at Jefferson Laboratory and in two-photon collisions at CLEO, Belle, and BaBar [152]. Hadronic exclusive processes are closely related to exclusive hadronic B decays, processes which are essential for determining the CKM phases and the physics of CP violation. The universal light-front wavefunctions which control hard exclusive processes such as form factors, deeply virtual Compton scattering, high momentum transfer photoproduction, and two-photon processes, are also required for computing exclusive heavy hadron decays [153, 154, 155, 156], such as $B \to K\pi$, $B \to \ell\nu\pi$, and $B \to Kp\overline{p}$ [157]. The same physics issues, including color transparency, hadron helicity rules, and the question of dominance of leading-twist perturbative QCD mechanisms enter in both realms of physics.

The data for virtually all measured hard scattering processes appear to be consistent with the conformal predictions of QCD. For example, one also sees the onset of the predicted perturbative QCD scaling behavior for exclusive nuclear amplitudes such as deuteron photodisintegration (Here $n = 1+6+3+3 = 13$.) $s^{11}\frac{d\sigma}{dt}(\gamma d \to pn) \sim$ constant at fixed CM angle. The measured deuteron form factor and the deuteron photodisintegration cross section appear to follow the leading-twist QCD predictions at large momentum transfers in the few GeV region [158, 159, 160]. A comparison of the data with the QCD predictions is shown in Fig. 8.

Another application to exclusive nuclear processes is the approach to scaling of the deuteron form factor $[Q^2]^5\sqrt{A(Q^2)} \to$ const observed at SLAC and Jefferson laboratory at high Q^2. These scaling laws reflects the underlying scaling of the nucleon-nucleon interaction and the nuclear force at short distances. The phenomenological successes provide further evidence for the dominance of leading-twist quark-gluon subprocesses and the near conformal behavior of the QCD coupling. As discussed above, the evidence that the running coupling has constant fixed-point behavior, which together with BLM scale fixing, could help explain the near conformal scaling behavior of the fixed-CM angle cross sections. The angular distribution of hard exclusive processes is generally consistent with quark interchange, as predicted from large N_C considerations.

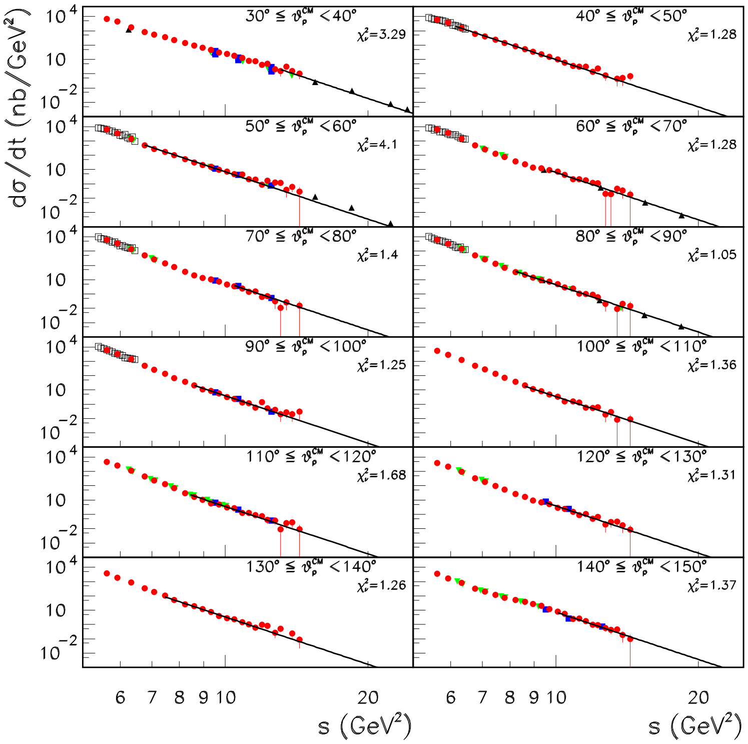

Figure 8: Fits of the cross sections $d\sigma/dt$ to s^{-11} for $P_T \geq P_T^{th}$ and proton angles between 30° and 150° (solid lines). Data are from CLAS (full/red circles), Mainz(open/black squares), SLAC (full-down/green triangles), JLab Hall A (full/blue squares) and Hall C (full-up/black triangles). Also shown in each panel is the χ^2_ν value of the fit. From Ref. [160].

10 The Evolution of the Deuteron Distribution Amplitude and Hidden Color

In this section I will review an analysis by Chueng Ji, Peter Lepage, and myself which shows how the asymptotic behavior of the deuteron form factor at large momentum transfer and the evolution of the deuteron six-quark distribution amplitude at short distances can be computed systematically as an expansion in $\alpha_s(Q^2)$ [150]. The results agree with the operator product expansion as well as the conformal scaling implied by the AdS/CFT correspondence. As we shall see, the QCD predictions appear to be in remarkable agreement with experiment for $Q^2 \gtrsim 1$ GeV^2 particularly when expressed in terms of the deuteron reduced form factor. This provides a good check on the six-quark description of the deuteron at short distances as well as the scale invariance of the elastic quark-quark scattering amplitude. I will also discuss how the dominance of the hidden color amplitudes at short distances also provides an explanation for the repulsive behavior of the nucleon-nucleon potential at small inter-nucleon separation.

Hadronic form factors in QCD at large momentum transfer $Q^2 = \vec{q}^{\,2} - q_0^2$ can be written in a factorized form where all nonperturbative effects are incorporated into process-independent distribution amplitudes $\phi_H(x_i, Q)$, computed from the equal $\tau = t+z$, six-quark valence wave function at small relative quark transverse separation $b^i_\perp \sim O(1/Q)$. The $x_i = (k^0+k^3)_i/(p^0+p^3)$ are the light-front longitudinal momentum fractions with $\sum_{i=1}^n x_i = 1$. In the case of the deuteron, only the six-quark Fock state needs to be considered for the purpose of computing a hard scattering amplitude since in a physical gauge any additional quark or gluon forced to absorb large momentum transfer yields a power law suppressed contribution to the form factor. The deuteron form factor can then be written as a convolution

$$F_d(Q^2) = \int_0^1 [dx][dy]\phi_d^\dagger(y, Q)\, T_H^{6_q+\gamma^*\to 6_q}(x, y, Q)\phi_d(x, Q)\ , \tag{17}$$

where the hard scattering amplitude

$$T_H^{6_q+\gamma^*\to 6_q} = \left[\frac{\alpha_s(Q^2)}{Q^2}\right]^5 t(x, y)\left[1 + O(\alpha_s(Q^2))\right] \tag{18}$$

gives the probability amplitude for scattering six quarks collinear with the initial to the final deuteron momentum and

$$\phi_d(x_i, Q) \propto \int^{k_{\perp\, i}<Q} \left[d^{\,2}k_\perp\right]\ \psi_{qqq\,qqq}(x_i, \vec{k}_{\perp\, i}) \tag{19}$$

gives the probability amplitude for finding the quarks with longitudinal momentum fractions x_i in the deuteron wavefunction collinear up to the scale Q. Because the coupling of the gauge gluon is helicity-conserving and the fact that $\phi_d(x_i, Q)$ is the $L_z = 0$ projection of the deuteron wavefunction, hadron helicity is conserved: The dominant form factor corresponds to $\sqrt{A}(Q^2)$; *i.e.*, $h = h' = 0$.

The distribution amplitude $\phi_d(x_i, Q)$ is the basic deuteron wave function which controls high momentum transfer exclusive reactions in QCD. The logarithmic Q^2 dependence Of ϕ_d is determined by an evolution equation computed from perturbative quark-quark scattering kernels at large momentum transfer, or equivalently, by the operator product expansion at short distances and the renormalization group [64, 161, 149].

The QCD prediction for the leading helicity-zero deuteron form factor then has the form [162, 163]

$$F_d(q^2) = \left[\frac{\alpha_s(Q^2)}{Q^2}\right]^5 \sum_{m,n} d_{mn}\left(\ell n\,\frac{Q^2}{\Lambda^2}\right)^{-\gamma_n^d-\gamma_m^d}\ \left[1 + O\left(\alpha_s(Q^2),\, \frac{m}{Q}\right)\right]\ , \tag{20}$$

where the main dependence $[\alpha_s(Q^2)/Q^2]^5$ comes from the hard-gluon exchange amplitude T_H. The anomalous dimensions γ_n^d are calculated from the evolution equations for $\psi_d(x_i, Q)$.

The evolution equation for six quark systems in which the constituents have the light-front longitudinal momentum fractions x_i $(i = 1, 2, \ldots, 6)$ can be obtained from a generalization of the proton (three quark) case [64, 161, 149]. A nontrivial extension is the calculation of the color factor, C_d, of six quark systems. Since in leading order only pair-wise interactions, with transverse momentum Q, occur between quarks, the evolution equation for the six-quark system becomes $\{[dy] = \delta(1 - \sum_{i=1}^{6} y_i) \prod_{i=1}^{6} dy_i$, $C_F = (n_c^2 - 1)/2n_c = (4/3), \beta = 11 - (2/3)n_f$, and n_f is the effective number of flavors)

$$\prod_{k=1}^{6} x_k \left[\frac{\partial}{\partial\xi} + \frac{3C_F}{\beta}\right] \widetilde{\Phi}(x_i, Q) = -\frac{C_d}{\beta} \int_0^1 [dy]\, V(x_i, y_i) \widetilde{\Phi}(y_i, Q)\,, \tag{21}$$

where the factor 3 in the square bracket comes from the renormalization of the six quark field. In Eq. (21) we have defined $\Phi(x_i, Q) = \prod_{k=1}^{6} x_k \widetilde{\Phi}(x_i, Q)$. The evolution is in the variable

$$\xi(Q^2) = \frac{\beta}{4\pi} \int_{Q_0^2}^{Q^2} \frac{dk^2}{k^2}\, \alpha_s(k^2) \sim \ell n \left(\frac{\ell n \frac{Q^2}{\Lambda^2}}{\ell n \frac{Q_0^2}{\Lambda^2}} \right) \,. \tag{22}$$

By summing over interactions between quark pairs $\{i, j\}$ due to exchange of a single gluon, $V(x_i, y_i) = V(y_i, x_i)$ is given by

$$V(x_i, y_i) = 2 \prod_{k=1}^{6} x_k \sum_{i \neq j}^{6} \theta(y_i - x_i) \prod_{\ell \neq i,j}^{6} \delta(x_\ell - y_\ell)\, \frac{y_j}{x_j} \left(\frac{\delta_{h_i \bar{h}_j}}{x_i + x_j} + \frac{\Delta}{y_i - x_i} \right) \,, \tag{23}$$

where $\delta_{h_i \bar{h}_j} = 1(0)$ when the constituents' $\{i, j\}$ helicities are antiparallel (parallel). The infrared singularity at $x_i = y_i$ is cancelled by the factor $\Delta\widetilde{\Phi}(y_i, Q) = \widetilde{\Phi}(y_i, Q) - \widetilde{\Phi}(x_i, Q)$ since the deuteron is a color singlet.

The six-quark bound states have five independent color singlet components ($3 \times 3 \times 3 \times 3 \times 3 \times 3 \supset \underline{1} + \underline{1} + \underline{1} + \underline{1} + \underline{1}$). It can be shown in general that the color factor C_d is given by

$$C_d = \frac{1}{5}\, S_{ijk\ell mn}{}^{\alpha} \left(\frac{1}{2}\lambda_a\right)_{i'}{}^{i} \left(\frac{1}{2}\lambda_a\right)_{j'}{}^{j} S_{\alpha}^{i'j'k\ell mn} \,, \tag{24}$$

where $\lambda_a (a = 1, 2, \ldots, 8)$ are Gell-Mann matrices in $SU(3)^c$ group and $s_{ijk\ell mn}^{\alpha} (\alpha = 1, 2, \ldots, 5)$ are the five independent color singlet representations. We shall focus on results for the leading contribution to the distribution amplitude and form factor at large Q. Since the leading eigensolution to the evolution Eq. (21) turns out to be completely symmetric in its orbital dependence, the dominant asymptotic deuteron wavefunction is fixed by overall anti-symmetry to have spin-isospin symmetry $\{3\}_{TS}$ which is dual to its color symmetry $[222]_c$. Thus the coefficient for each c (and TS) component has equal weights:

$$\phi_{6_q}\left([222]_c \otimes \{33\}_{TS}\right) = \frac{1}{\sqrt{5}} \sum_{\alpha=1}^{5} (-1)^{\alpha} [222]_c{}^{\alpha} \{33\}_{TS}^{\alpha} \,. \tag{25}$$

Since the evolution potential is diagonal in isospin and spin, C_d is computed by the trace of the color representation. The color factor is $-2/3$ for the color antisymmetric pair $\{i,j\}$ and $+1/3$ for the color symmetric pair $\{i,j\}$. Since three color antisymmetric pairs $\{i,j\}$ and two color symmetric pairs $\{i,j\}$ exist in this state, the color factor is

$$C_d = \frac{1}{5}\left(-\frac{2}{3}\times 3 + \frac{1}{3}\times 2\right) = \frac{C_F}{5}\ . \tag{26}$$

To solve the evolution Eq. (21), we factorize the Q^2 dependence of $\widetilde{\Phi}(x_i,Q)$ as

$$\widetilde{\Phi}(x_i,Q) = \widetilde{\Phi}(x_i)\, e^{-\gamma\xi} = \widetilde{\Phi}(x_i)\ \left[\ell n\frac{Q^2}{\Lambda^2}\right]^{-\gamma}\ , \tag{27}$$

where the eigenvalues of γ will provide the anomalous dimensions γ_n. The leading anomalous dimension γ_0 [corresponding to the eigenfunction $\widetilde{\Phi}(x_i)=1$] is

$$\gamma_0 = \frac{3C_F}{\beta} + \frac{C_d}{\beta}\sum_{i\neq j}^{6}\delta_{h_i\bar{h}_j}\ , \tag{28}$$

so that the asymptotically dominant result for the helicity zero deuteron is given by $\gamma_0 = (6/5)(C_F/\beta)$.

Note that in order to have logarithmic evolution of the deuteron distribution amplitude, the six-quark valence light-front wavefunction must fall nominally as $\psi_{qqqqqq/d}(x_i,k_{\perp i}) \simeq [\frac{1}{k_\perp^2}]^5$. This is also the prediction of conformal invariance and the AdS/CFT correspondence. More generally, consistency with the operator product expansion for the moments of the distribution amplitude requires the power law fall off $\psi_n(x_i,k_{\perp i}) \simeq [\frac{1}{k_\perp^2}]^{n-1}$ for all n-parton LFWFs with $L_z=0$.

At high Q^2 the deuteron form factor is sensitive to wavefunction configurations where all six quarks overlap within an impact separation $b_{\perp i} < \mathcal{O}(1/Q)$. Since the deuteron form factor contains the probability amplitudes for the proton and neutron to scatter from $p/2$ to $p/2+q/2$, it is natural to define the reduced deuteron form factor[163, 150]

$$f_d(Q^2) \equiv \frac{F_d(Q^2)}{F_{1N}\left(\frac{Q^2}{4}\right)\,F_{1N}\left(\frac{Q^2}{4}\right)}. \tag{29}$$

The effect of nucleon compositeness is removed from the reduced form factor. Since the leading anomalous dimensions of the nucleon distribution amplitude is $C_F/2\beta$, the QCD prediction for the asymptotic Q^2 behavior of $f_d(Q^2)$ is

$$f_d(Q^2) \sim \frac{\alpha_s(Q^2)}{Q^2}\left(\ell n\frac{Q^2}{\Lambda^2}\right)^{(2/5)\,C_F/\beta}\ , \tag{30}$$

where $(2/5)(C_F/\beta) = -(8/145)$ for $n_f=2$.

QCD thus predicts essentially the same scaling law for the reduced deuteron form factor as a meson form factor. This scaling is consistent with experiment for $Q^2 > 1$ GeV^2. In fact as seen in Fig. 9, the deuteron reduced form factor contains two components: (1) a fast-falling component characteristic of nuclear binding with probability 85%, and (2) a hard contribution falling as a monopole with a scale of order 0.5 GeV with probability 15%. The normalization of the deuteron form factor observed at large Q^2 [164], as well as the presence of two mass scales in the scaling behavior of the reduced deuteron form factor [163] thus suggests sizable hidden-color Fock state contributions such as $|(uud)_{8_C}(ddu)_{8_C}\rangle$ with probability of order 15% in the deuteron wavefunction [165].

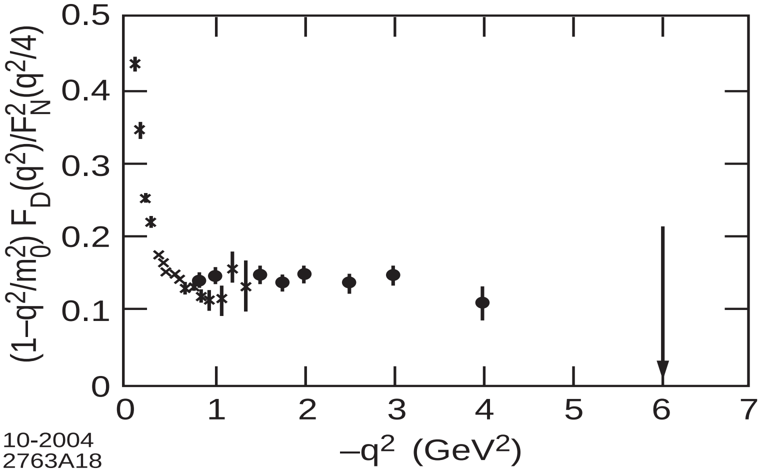

Figure 9: Reduced Deuteron Form Factor showing the scaling predicted by perturbative QCD and conformal scaling. The data show two regimes: a fast-falling behavior at small Q^2 characteristic of normal nuclear binding, and a hard scattering regime with monopole fall-off controlled by the scale $m_0^2 = 0.28$ GeV^2. The latter contribution is attributable to non-nucleonic hidden-color components of the deuteron's six-quark Fock state. From Ref. [163].

In general, one would expect corrections from the leading twist QCD predictions from higher-twist effects (*e.g.*, mass and $k_\perp$ smearing) and higher-order contributions in $\alpha_s(Q^2)$, as well as nonleading anomalous dimensions. However, the agreement of the data with simple $Q^2 f_d(Q^2) \sim$ const. behavior for $Q^2 > 1/2$ GeV^2 implies that, unless there is a fortuitous cancellations, all of the scale-breaking effects are small, and the present QCD perturbation calculations are viable and applicable even in the nuclear physics domain. The lack of deviation from the QCD parametrization suggests that the parameter Λ in Eq. (30) is small. Alternatively, this can be taken as evidence for fixed point behavior of the QCD coupling in the infrared. A comparison with a standard definition such as $\Lambda_{\overline{MS}}$ would require a calculation of next-to-leading effects. A more definitive check of QCD can be made by calculating the normalization of $f_d(Q^2)$ from a perturbative calculation of T_H and the evolution of the deuteron wave function to short distances. It is also important to confirm experimentally that the $h = h' = 0$ form factor is indeed dominant.

Note that the deuteron wave function which contributes to the asymptotic limit of the form factor is the totally antisymmetric wave function corresponding to the orbital Young symmetry given by [6] and isospin $(T)+$ spin (S) Young symmetry given by $\{33\}$. The deuteron state with this symmetry is related to the NN, $\Delta\Delta$, and hidden-color (CC) physical bases, for both the $(TS) = (01)$ and (10) cases, by the formula

$$\psi_{[6]\{33\}} = \left(\frac{1}{9}\right)^{1/2} \psi_{NN} + \left(\frac{4}{45}\right)^{1/2} \psi_{\Delta\Delta} + \left(\frac{4}{5}\right)^{1/2} \psi_{CC} \ . \tag{31}$$

Thus the physical deuteron state, which is mostly ψ_{NN} at large distance, must evolve to the $\psi_{[6]\{33\}}$ state when the six-quark transverse separations $b^i_\perp \leq O(1/Q) \to 0$. Since this state is 80% hidden color, the deuteron wave functions cannot be described by the nucleonic degrees of freedom in this domain. The fact that the six-quark color-singlet state inevitably evolves in QCD to a dominantly hidden-color configuration at small transverse separation also has implications for the form of the nucleon-nucleon potential, which can be considered as one component in a coupled-channel system. As the two nucleons approach each other, the system must do work in order to change the six-quark state to a dominantly hidden-color configuration; *i.e.*, QCD requires that the nucleon-nucleon potential must be repulsive at short distances [166].

Thus a rigorous prediction of QCD is the "hidden color" of nuclear wavefunctions at short distances. QCD predicts that nuclear wavefunctions contain "hidden color" [167, 150] components: color configurations not dual to the usual nucleonic degrees of freedom. In general, the six-quark wavefunction of a deuteron is a mixture of five different color-singlet states. The dominant color configuration at large distances corresponds to the usual proton-neutron bound state where transverse momenta are of order $\vec{k}^2 \sim 2M_d\epsilon_{BE}$. However, at small impact space separation, all five Fock color-singlet components eventually acquire equal weight, *i.e.*, the deuteron wavefunction evolves to 80% hidden color.

10.1 Hadron Helicity Conservation

The distribution amplitudes are $L_z = 0$ projections of the LF wavefunction, and the sum of the spin projections of the valence quarks must equal the J_z of the parent hadron. Higher orbital angular momentum components lead to power-law suppressed exclusive amplitudes [64, 30]. Since quark masses can be neglected at leading twist in T_H, one has quark helicity conservation, and thus, finally, hadron-helicity conservation: the sum of initial hadron helicities equals the sum of final helicities. In particular, since the hadron-helicity violating Pauli form factor is computed from states with $\Delta L_z = \pm 1$, PQCD predicts $F_2(Q^2)/F_1(Q^2) \sim 1/Q^2$ [modulo logarithms]. A detailed analysis shows that the asymptotic fall-off takes the form $F_2(Q^2)/F_1(Q^2) \sim \log^2 Q^2/Q^2$ [168]. One can also construct other models [91] incorporating the leading-twist perturbative QCD prediction which are consistent with the JLab polarization transfer data [169] for the ratio of proton Pauli and Dirac form factors. This analysis can also be extended to study the spin structure of scattering amplitudes at large transverse momentum and other processes which are dependent on the scaling and orbital angular momentum structure of light-front wavefunctions. Recently, Afanasev, Carlson, Chen, Vanderhaeghen, and I [170] have shown that the interfering two-photon exchange contribution to elastic electron-proton scattering, including inelastic intermediate states, can account for the discrepancy between Rosenbluth and Jefferson Lab spin transfer polarization data [169].

10.2 Timelike Form Factors

A crucial prediction of models for proton form factors is the relative phase of the timelike form factors, since this can be measured from the proton single spin symmetries in $e^+e^- \to p\overline{p}$ or $p\overline{p} \to \ell\overline{\ell}$ [171]. Carl Carlson, John Hiller, Dae Sung Hwang and I [171] have shown that measurements of the proton's polarization strongly discriminate between the analytic forms of models which fit the proton form factors in the spacelike region. In particular, the single-spin asymmetry normal to the scattering plane measures the relative phase difference between the timelike G_E and G_M form factors. The dependence on proton polarization in the timelike region is expected to be large in most models, of the order of several tens of percent. The continuation of the spacelike form factors to the timelike domain $t = s > 4M_p^2$ is very sensitive to the analytic form of the form factors; in particular it is very sensitive to the form of the PQCD predictions including the corrections to conformal scaling. The forward-backward $\ell^+\ell^-$ asymmetry can measure the interference of one-photon and two-photon contributions to $\overline{p}p \to \ell^+\ell^-$.

11 Complications from Final-State Interactions

Although it has been more than 35 years since the discovery of Bjorken scaling [172] in electroproduction [173], there are still many issues in deep-inelastic lepton scattering and Drell-Yan reactions which are only now being understood from a fundamental basis in QCD.

It is usually assumed—following the parton model—that the leading-twist structure functions measured in deep inelastic lepton-proton scattering are simply the probability distributions for finding quarks and gluons in the target nucleon. In fact, gluon exchange between the fast, outgoing quarks and the target spectators effects the leading-twist structure functions in a profound way, leading to diffractive leptoproduction processes, shadowing of nuclear structure functions, and target spin asymmetries.

As I shall discuss in this section, the final-state interactions from gluon exchange between the outgoing quark and the target spectator system lead to single-spin asymmetries in semi-inclusive deep inelastic lepton-proton scattering at leading twist in perturbative QCD; *i.e.*, the rescattering corrections of the struck quark with the target spectators are not power-law suppressed at large photon virtuality Q^2 at fixed x_{bj} [174] The final-state interaction from gluon exchange occurring immediately after the interaction of the current also produces a leading-twist diffractive component to deep inelastic scattering $\ell p \to \ell' p' X$ corresponding to color-singlet exchange with the target system; this in turn produces shadowing and anti-shadowing of the nuclear structure functions [87, 175]. In addition, one can show that the pomeron structure function derived from diffractive DIS has the same form as the quark contribution of the gluon structure function [176]. The final-state interactions occur at a short light-front time $\Delta\tau \simeq 1/\nu$ after the virtual photon interacts with the struck quark, producing a nontrivial phase. Here $\nu = p \cdot q/M$ is the laboratory energy of the virtual photon. Thus none of the above phenomena is contained in the target light-front wave functions computed in isolation. In particular, the shadowing of nuclear structure functions is due to destructive interference effects from leading-twist diffraction of the virtual photon, physics not included in the nuclear light-front wave functions. Thus the structure functions measured in deep inelastic lepton scattering are affected by final-state rescattering, modifying their connection to light-front probability distributions. As an alternative formalism, one can augment the light-front wave functions with a gauge link corresponding to an external field created by the virtual photon $q\bar{q}$ pair current [177, 178]. Such a gauge link is process dependent [179], so the resulting augmented LFWFs are not universal [87, 177, 180]. Such rescattering corrections are not contained in the target light-front wave functions computed in isolation.

Single-spin asymmetries in hadronic reactions provide a remarkable window to QCD mechanisms at the amplitude level. In general, single-spin asymmetries measure the correlation of the spin projection of a hadron with a production or scattering plane [181]. Such correlations are odd under time reversal, and thus they can arise in a time-reversal invariant theory only when there is a phase difference between different spin amplitudes. Specifically, a nonzero correlation of the proton spin normal to a production plane measures the phase difference between two amplitudes coupling the proton target with $J^z_p = \pm\frac{1}{2}$ to the same final-state. The calculation requires the overlap of target light-front wavefunctions with different orbital angular momentum: $\Delta L^z = 1$; thus a single-spin asymmetry (SSA) provides a direct measure of orbital angular momentum in the QCD bound state.

The shadowing and antishadowing of nuclear structure functions in the Gribov-Glauber picture is due to the destructive and constructive coherence, respectively, of amplitudes arising from the multiple-scattering of quarks in the nucleus. The effective quark-nucleon scattering amplitude includes Pomeron and Odderon contributions from multi-gluon exchange as well as Reggeon quark exchange contributions [175]. The multiscattering nuclear processes from Pomeron, Odderon and pseudoscalar Reggeon exchange leads to shadowing and antishadowing of the electromagnetic nuclear structure functions in agreement with measurements. An important conclusion is that antishadowing is nonuniversal—different for quarks and antiquarks and different for strange quarks versus light quarks. This picture thus leads to substantially different nuclear effects for charged and neutral currents, particularly in anti-neutrino reactions, thus affecting the extraction of the weak-mixing angle $\sin^2\theta_W$ and the constant ρ_o which are determined from the ratios of charged and neutral current contributions in deep inelastic neutrino and anti-neutrino scattering. In recent work, Schmidt, Yang, and I [182] have shown that a substantial part of the difference between the standard model prediction and the anomalous NuTeV result [183] for $\sin^2\theta_W$ could be due to the different behavior of nuclear antishadowing for charged and neutral currents. Detailed measurements of the nuclear dependence of charged, neutral and electromagnetic DIS processes are needed to establish the distinctive phenomenology of shadowing and antishadowing and to make the NuTeV results definitive.

11.1 The Paradox of Diffractive Deep Inelastic Scattering

A remarkable feature of deep inelastic lepton-proton scattering at HERA is that approximately 10% events are diffractive [184, 185, 186]: the target proton remains intact and there is a large rapidity gap between the proton and the other hadrons in the final state. These diffractive deep inelastic scattering (DDIS) events can be understood most simply from the perspective of the color-dipole model [187]: the $q\overline{q}$ Fock state of the high-energy virtual photon diffractively dissociates into a diffractive dijet system. The color-singlet exchange of multiple gluons between the color dipole of the $q\overline{q}$ and the quarks of the target proton leads to the diffractive final state. The same hard pomeron exchange also controls diffractive vector meson electroproduction at large photon virtuality [188]. One can show by analyticity and crossing symmetry that amplitudes with $C = +$ hard-pomeron exchange have a nearly imaginary phase.

This observation presents a paradox: deep inelastic scattering is usually discussed in terms of the parton model. If one chooses the conventional parton model frame where the photon light-front momentum is negative $q+ = q^0 + q^z < 0$, then the virtual photon cannot produce a virtual $q\overline{q}$ pair. Instead, the virtual photon always interacts with a quark constituent with light-front momentum fraction $x = \frac{k^+}{p^+} = x_{bj}$. If one chooses light-front gauge $A^+ = 0$, then the gauge link associated with the struck quark (the Wilson line) becomes unity. Thus the struck "current" quark experiences no final-state interactions. The light-front wavefunctions $\psi_n(x_i, k_{\perp i}$ of the proton which determine the quark probability distributions $q(x, Q)$ are real since the proton is stable. Thus it appears impossible to generate the required imaginary phase, let alone the large rapidity gaps associated with of DDIS.

This paradox was resolved by Paul Hoyer, Nils Marchal, Stephane Peigne, Francesco Sannino and myself [87]. It is helpful to consider the case where the virtual photon interacts with a strange quark – the $s\overline{s}$ pair is assumed to be produced in the target by gluon splitting. In the case of Feynman gauge, the struck s quark continues to interact in the final state via gluon exchange as described by the Wilson line. The final-state interactions occur at a light-front time $\Delta\tau \simeq 1/\nu$ after the virtual photon interacts with the struck quark. When one integrates over the nearly-on-shell intermediate state, the amplitude acquires an imaginary part. Thus the rescattering of the quark produces a separated color-singlet $s\overline{s}$ and an imaginary phase.

In contrast, in the case of the light-front gauge $A^+ = n \cdot A = 0$, one must consider the final state interactions of the (unstruck) $\overline{s}$ quark. light-front gauge is singular—in particular, the gluon propagator

$$d_{LC}^{\mu\nu}(k) = \frac{i}{k^2 + i\varepsilon}\left[-g^{\mu\nu} + \frac{n^\mu k^\nu + k^\mu n^\nu}{n \cdot k}\right] \tag{32}$$

has a pole at $k^+ = 0$ which requires an analytic prescription. In final-state scattering involving nearly on-shell intermediate states, the exchanged momentum k^+ is of $O\,(1/\nu)$ in the target rest frame, which enhances the second term in the propagator. This enhancement allows rescattering to contribute at leading twist even in LC gauge. Thus the rescattering contribution survives in the Bjorken limit because of the singular behavior of the propagator of the exchanged gluon at small k^+ in $A^+ = 0$ gauge. The net result is gauge invariant and identical to the color dipole model calculation.

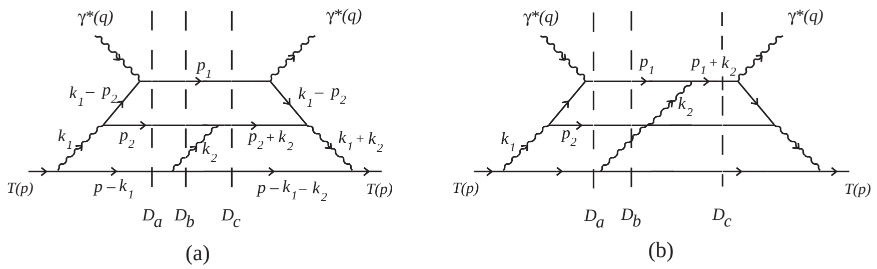

Figure 10: Two types of final state interactions. (a) Scattering of the antiquark (p_2 line), which in the aligned jet kinematics is part of the target dynamics. (b) Scattering of the current quark (p_1 line). For each light-front time-ordered diagram, the potentially on-shell intermediate states—corresponding to the zeroes of the denominators D_a, D_b, D_c—are denoted by dashed lines.

The calculation of the rescattering effects on DIS in Feynman and light-front gauge through three loops is given in detail for a simple Abelian model in Ref. [87]. Figure 10 illustrates two LCPTH diagrams which contribute to the forward $\gamma^* T \to \gamma^* T$ amplitude, where the target T is taken to be a single quark. In the aligned jet kinematics the virtual photon fluctuates into a q$\overline{\text{q}}$ pair with limited transverse momentum, and the (struck) quark takes nearly all the longitudinal momentum of the photon. The initial q and $\overline{\mathrm{q}}$ momenta are denoted p_1 and $p_2 - k_1$, respectively. The result is most easily expressed in eikonal form in terms of transverse distances r_T, R_T conjugate to p_{2T}, k_T. The DIS cross section can be expressed as

$$Q^4 \frac{d\sigma}{dQ^2\, dx_B} = \frac{\alpha_{\rm em}}{16\pi^2} \frac{1-y}{y^2} \frac{1}{2M\nu} \int \frac{dp_2^-}{p_2^-}\, d^2\vec{r}_T\, d^2\vec{R}_T\, |\tilde{M}|^2 \tag{33}$$

where

$$|\tilde{M}(p_2^-, \vec{r}_T, \vec{R}_T)| = \left| \frac{\sin\left[g^2\, W(\vec{r}_T, \vec{R}_T)/2\right]}{g^2\, W(\vec{r}_T, \vec{R}_T)/2} \tilde{A}(p_2^-, \vec{r}_T, \vec{R}_T) \right| \tag{34}$$

is the resummed result. The Born amplitude is

$$\tilde{A}(p_2^-, \vec{r}_T, \vec{R}_T) = 2eg^2 MQp_2^-\, V(m_{PhysLett} r_T) W(\vec{r}_T, \vec{R}_T) \tag{35}$$

where $m_{PhysLett}^2 = p_2^- M x_B + m^2$ and

$$V(m\, r_T) \equiv \int \frac{d^2\vec{p}_T}{(2\pi)^2} \frac{e^{i\vec{r}_T\cdot\vec{p}_T}}{p_T^2 + m^2} = \frac{1}{2\pi} K_0(m\, r_T). \tag{36}$$

The rescattering effect of the dipole of the $\mathrm{q}\overline{\mathrm{q}}$ is controlled by

$$W(\vec{r}_T, \vec{R}_T) \equiv \int \frac{d^2\vec{k}_T}{(2\pi)^2} \frac{1 - e^{i\vec{r}_T\cdot\vec{k}_T}}{k_T^2} e^{i\vec{R}_T\cdot\vec{k}_T} = \frac{1}{2\pi} \log\left(\frac{|\vec{R}_T + \vec{r}_T|}{R_T} \right). \tag{37}$$

The fact that the coefficient of $\tilde{A}$ in is less than unity for all $\vec{r}_T, \vec{R}_T$ shows that the rescattering corrections reduce the cross section in analogy to nuclear shadowing.

A new understanding of the role of final-state interactions in deep inelastic scattering has thus emerged. The final-state interactions from gluon exchange occurring immediately after the interaction of the current produce a leading-twist diffractive component to deep inelastic scattering $\ell p \to \ell' p' X$ due to the color-singlet exchange with the target system. This rescattering is described in the Feynman gauge by the path-ordered exponential (Wilson line) in the expression for the parton distribution function of the target. The multiple scattering of the struck parton via instantaneous interactions in the target generates dominantly imaginary diffractive amplitudes, giving rise to an effective "hard pomeron" exchange. The presence of a rapidity gap between the target and diffractive system requires that the target remnant emerges in a color-singlet state; this is made possible in any gauge by the soft rescattering of the final-state $s - \overline{s}$ system.

11.2 Diffractive Deep Inelastic Reactions and Rescattering

Rikard Enberg, Paul Hoyer, Gunnar Ingelman and I have recently discussed some further aspects of the QCD dynamics of diffractive deep inelastic scattering [176]. We show that the quark structure function of the effective hard pomeron has the same form as the quark contribution of the gluon structure function. The hard pomeron is not an intrinsic part of the proton; rather it must be considered as a dynamical effect of the lepton-proton interaction.

Our QCD-based picture also applies to diffraction in hadron-initiated processes. The rescattering is different in virtual photon- and hadron-induced processes due to the different color environment, which accounts for the observed non-universality of diffractive parton distributions. In the hadronic case the color flow at tree level can involve color-octet as well as color-triplet separation. Multiple scattering of the quarks and gluons can set up a variety of different color singlet domains. This framework also provides a theoretical basis for the phenomenologically successful Soft Color Interaction (SCI) model which includes rescattering effects and thus generates a variety of final states with rapidity gaps.

11.3 Origin of Nuclear Shadowing and Antishadowing

The physics of nuclear shadowing in deep inelastic scattering can be most easily understood in the laboratory frame using the Glauber-Gribov picture [189, 190, 191]. The virtual photon, W, or Z^0 produces a quark-antiquark color-dipole pair which can interact diffractively or inelastically on the nucleons in the nucleus. The destructive interference of diffractive amplitudes from pomeron exchange on the upstream nucleons then causes shadowing of the virtual photon interactions on the back-face nucleons [192, 193, 194, 195, 196, 197, 198]. The Bjorken-scaling diffractive interactions on the nucleons in a nucleus thus leads to the shadowing (depletion at small x_{bj}) of the nuclear structure functions.

As emphasized by Ioffe [195], the coherence between processes which occur on different nucleons at separation L_A requires small Bjorken $x_B : 1/Mx_B = 2\nu/Q^2 \geq L_A$. The coherence between different quark processes is also the basis of saturation phenomena in DIS and other hard QCD reactions at small x_B [199], and coherent multiple parton scattering has been used in the analysis of $p+A$ collisions in terms of the perturbative QCD factorization approach [200]. An example of the interference of one- and two-step processes in deep inelastic lepton-nucleus scattering illustrated in Fig. 11.

An important aspect of the shadowing phenomenon is that the diffractive contribution $\gamma^* N \to X N'$ to deep inelastic scattering (DDIS) where the nucleon N_1 in Fig. 11 remains intact is a constant fraction of the total DIS rate, confirming that it is a leading-twist contribution. The Bjorken scaling of DDIS has been observed at HERA [185, 201, 202]. As shown in Ref. [87], the leading-twist contribution to DDIS arises in QCD in the usual parton model frame when one includes the nearly instantaneous gluon exchange final-state interactions of the struck quark with the target spectators. The same final state interactions also lead to leading-twist single-spin asymmetries in semi-inclusive DIS [174]. Thus the shadowing of nuclear structure

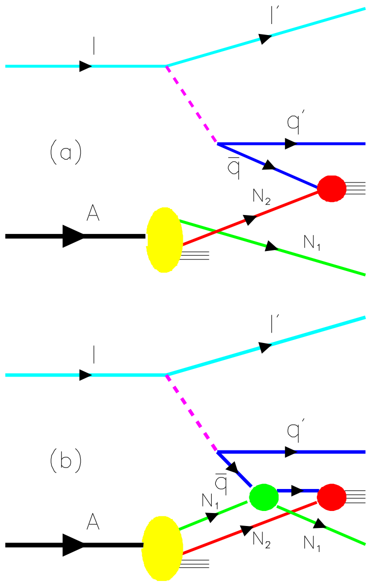

Figure 11: The one-step and two-step processes in DIS on a nucleus. If the scattering on nucleon N_1 is via pomeron exchange, the one-step and two-step amplitudes are opposite in phase, thus diminishing the $\overline{q}$ flux reaching N_2. This causes shadowing of the charged and neutral current nuclear structure functions.

functions is also a leading-twist effect.

It was shown in Ref. [175] that if one allows for Reggeon exchanges which leave a nucleon intact, then one can obtain *constructive* interference among the multi-scattering amplitudes in the nucleus. A Bjorken-scaling contribution to DDIS from Reggeon exchange has in fact also been observed at HERA [185, 202]. The strength and energy dependence of the $C = +$ Reggeon $t-$channel exchange contributions to virtual Compton scattering is constrained by the Kuti-Weisskopf [203] behavior $F_2(x) \sim x^{1-\alpha_R}$ of the non-singlet electromagnetic structure functions at small x. The phase of the Reggeon exchange amplitude is determined by its signature factor. Because of this phase structure [175], one obtains constructive interference and *antishadowing* of the nuclear structure functions in the range $0.1 < x < 0.2$ – a pronounced excess of the nuclear cross section with respect to nucleon additivity [204].

In the case where the diffractive amplitude on N_1 is imaginary, the two-step process has the phase $i \times i = -1$ relative to the one-step amplitude, producing destructive interference. (The second factor of i arises from integration over the quasi-real intermediate state.) In the case where the diffractive amplitude on N_1 is due to $C = +$ Reggeon exchange with intercept $\alpha_R(0) = 1/2$, for example, the phase of the two-step amplitude is $\frac{1}{\sqrt{2}}(1-i) \times i = \frac{1}{\sqrt{2}}(i+1)$ relative to the one-step amplitude, thus producing constructive interference and antishadowing.

The effective quark-nucleon scattering amplitude includes Pomeron and Odderon contributions from multi-gluon exchange as well as Reggeon quark-exchange contributions [175]. The coherence of these multiscattering nuclear processes leads to shadowing and antishadowing of the electromagnetic nuclear structure functions in agreement with measurements. The Reggeon contributions to the quark scattering amplitudes depend specifically on the quark flavor; for example the isovector Regge trajectories couple differently to u and d quarks. The s and $\overline{s}$ couple to yet different Reggeons. This implies distinct anti-shadowing effects for each quark and antiquark component of the nuclear structure function. Ivan Schmidt, Jian-Jun Yang, and I [205] have shown that this picture leads to substantially different antishadowing for charged and neutral current reactions.

Figures 12–13 illustrate the individual quark q and anti-quark $\overline{q}$ contributions to the ratio of the iron to nucleon structure functions $R = F_2^A/F_2^{N_0}$ in a model calculation where the Reggeon contributions are constrained by the Kuti-Weisskopf behavior [203] of the nucleon structure functions at small x_{bj}. Because the strange quark distribution is much smaller than u and d quark distributions, the strange quark contribution to the ratio is very close to 1 although s^A/s^{N_0} may significantly deviate from 1.

Our analysis leads to substantially different nuclear antishadowing for charged and neutral current reactions; in fact, the neutrino and antineutrino DIS cross sections are each modified in different ways due to the various allowed Regge exchanges. The non-universality of nuclear effects will modify the extraction of the weak-mixing angle $\sin^2\theta_W$, particularly because of the strong nuclear effects for the F_3 structure function. The shadowing and antishadowing of the strange quark structure function in the nucleus can also be considerably different than that of the light quarks. We thus find that part of the anomalous NuTeV result [206] for $\sin^2\theta_W$ could be due to the non-universality of nuclear antishadowing for charged and neutral currents. Our picture also implies non-universality for the nuclear modifications of spin-dependent structure functions.

Thus the antishadowing of nuclear structure functions depends in detail on quark flavor. Careful measurements of the nuclear dependence of charged, neutral, and electromagnetic DIS processes are needed to establish the distinctive phenomenology of shadowing and antishadowing and to make the NuTeV results definitive. It is also important to map out the shadowing and antishadowing of each quark component of the nuclear structure functions to illuminate the underlying QCD mechanisms. Such studies can be carried out in semi-inclusive deep inelastic scattering for the electromagnetic current at Hermes and at Jefferson Laboratory by tagging the flavor of the current quark or by using pion and kaon-induced Drell-Yan reactions. A new determination of $\sin^2\theta_W$ is also expected from the neutrino scattering experiment NOMAD at CERN [207]. A systematic program of measurements of the nuclear effects in charged and neutral current reactions could also be carried out in high energy electron-nucleus colliders such as HERA and eRHIC, or by using high intensity

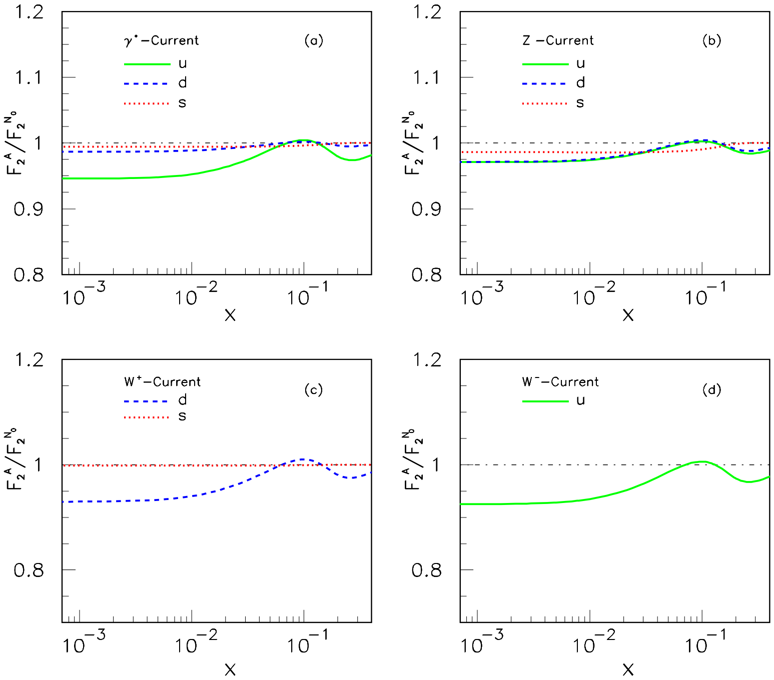

Figure 12: The quark contributions to the ratios of structure functions at $Q^2 = 1$ GeV^2. The solid, dashed and dotted curves correspond to the u, d and s quark contributions, respectively. This corresponds in our model to the nuclear dependence of the $\sigma(\overline{u} - A)$, $\sigma(\overline{d} - A)$, $\sigma(\overline{s} - A)$ cross sections, respectively. In order to stress the individual contribution of quarks, the numerator of the ratio $F_2^A/F_2^{N_0}$ shown in these two figures is obtained from the denominator by a replacement q^{N_0} into q^A for only the considered quark. As a result, the effect of antishadowing appears diminished.

neutrino beams [208].

11.4 Single-Spin Asymmetries from Final-State Interactions

Spin correlations provide a remarkably sensitive window to hadronic structure and basic mechanisms in QCD. Among the most interesting polarization effects are single-spin azimuthal asymmetries in semi-inclusive deep inelastic scattering, representing the correlation of the spin of the proton target and the virtual photon to hadron production plane: $\vec{S}_p \cdot \vec{q} \times \vec{p}_H$ [209]. Such asymmetries are time-reversal odd, but they can arise in QCD through phase differences in different spin amplitudes.

Until recently, the traditional explanation of pion electroproduction single-spin asymmetries in semi-inclusive deep inelastic scattering is that they are proportional to the transversity distribution of the quarks in the hadron h_1 [210, 211, 212] convoluted with the transverse momentum dependent fragmentation (Collins) function $H_1^\perp$, the distribution for a transversely polarized quark to fragment into an unpolarized hadron

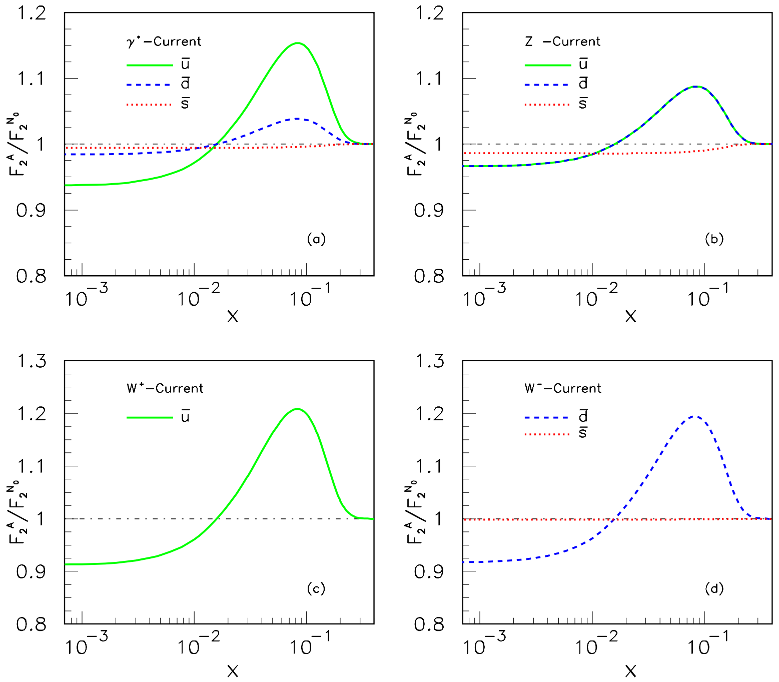

Figure 13: The anti-quark contributions to ratios of the structure functions at $Q^2 = 1$ GeV^2. The solid, dashed and dotted curves correspond to $\overline{u}$, $\overline{d}$ and $\overline{s}$ quark contributions, respectively. This corresponds in our model to the nuclear dependence of the $\sigma(u-A)$, $\sigma(d-A)$, $\sigma(s-A)$ cross sections, respectively. In order to stress the individual contribution of quarks, the numerator of the ratio $F_2^A/F_2^{N_0}$ shown in these two figures is obtained from the denominator by a replacement $\overline{q}^{N_0}$ into $\overline{q}^A$ for only the considered anti-quark.

with non-zero transverse momentum [213, 214, 215, 216, 217].

Dae Sung Hwang, Ivan Schmidt and I have showed that an alternative physical mechanism for the azimuthal asymmetries also exists [174, 218, 219]. The same QCD final-state interactions (gluon exchange) between the struck quark and the proton spectators which leads to diffractive events also can produce single-spin asymmetries (the Sivers effect) in semi-inclusive deep inelastic lepton scattering which survive in the Bjorken limit. This is illustrated in Fig. 14. In contrast to the SSAs arising from transversity and the Collins fragmentation function, the fragmentation of the quark into hadrons is not necessary; one predicts a correlation with the production plane of the quark jet itself $\vec{S}_p \cdot \vec{q} \times \vec{p}_q$.

The final-state interaction mechanism provides an appealing physical explanation within QCD of single-spin asymmetries. Remarkably, the same matrix element which determines the spin-orbit correlation $\vec{S} \cdot \vec{L}$ also produces the anomalous magnetic moment of the proton, the Pauli form factor, and the generalized parton distribution

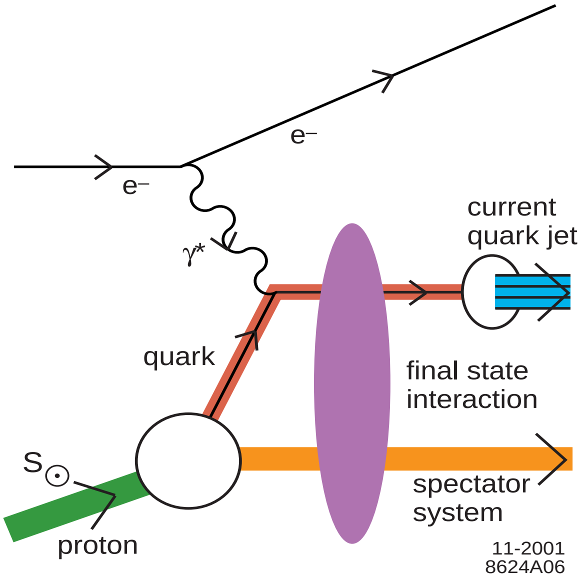

Figure 14: The origin of the Sivers effect in semi-inclusive deep inelastic scattering

E which is measured in deeply virtual Compton scattering. Physically, the final-state interaction phase arises as the infrared-finite difference of QCD Coulomb phases for hadron wave functions with differing orbital angular momentum. An elegant discussion of the Sivers effect including its sign has been given by Burkardt [220].

The final-state interaction effects can also be identified with the gauge link which is present in the gauge-invariant definition of parton distributions [218]. Even when the light-front gauge is chosen, a transverse gauge link is required. Thus in any gauge the parton amplitudes need to be augmented by an additional eikonal factor incorporating the final-state interaction and its phase [219, 177]. The net effect is that it is possible to define transverse momentum dependent parton distribution functions which contain the effect of the QCD final-state interactions.

A related analysis also predicts that the initial-state interactions from gluon exchange between the incoming quark and the target spectator system lead to leading-twist single-spin asymmetries in the Drell-Yan process $H_1 H_2^{\updownarrow} \to \ell^+ \ell^- X$ [179, 221]. Initial-state interactions also lead to a $\cos 2\phi$ planar correlation in unpolarized Drell-Yan reactions [222].

11.5 Calculations of Single-Spin Asymmetries in QCD

Hwang, Schmidt and I have calculated [174] the single-spin Sivers asymmetry in semi-inclusive electroproduction $\gamma^* p^{\updownarrow} \to HX$ induced by final-state interactions in a model of a spin-1/2 proton of mass M with charged spin-1/2 and spin-0 constituents of mass m and λ, respectively, as in the QCD-motivated quark-diquark model of a nucleon. The basic electroproduction reaction is then $\gamma^* p \to q(qq)_0$. In fact, the asymmetry comes from the interference of two amplitudes which have different proton spin, but couple to the same final quark spin state, and therefore it involves the interference of tree and one-loop diagrams with a final-state interaction. In this simple model the azimuthal target single-spin asymmetry $A_{UT}^{\sin\phi}$ is given by

$$\begin{aligned} A_{UT}^{\sin\phi} &= C_F \alpha_s(\mu^2) \, \frac{\Big(\, \Delta\, M + m \,\Big)\, r_\perp}{\Big[\, \Big(\, \Delta\, M + m \,\Big)^2 \; + \; \vec{r}_\perp^{\,2} \;\Big]} \\ &\times \; \Big[\, \vec{r}_\perp^{\,2} + \Delta(1-\Delta)(-M^2 + \frac{m^2}{\Delta} + \frac{\lambda^2}{1-\Delta}) \,\Big] \\ &\times \; \frac{1}{\vec{r}_\perp^{\,2}} \ln \frac{\vec{r}_\perp^{\,2} + \Delta(1-\Delta)(-M^2 + \frac{m^2}{\Delta} + \frac{\lambda^2}{1-\Delta})}{\Delta(1-\Delta)(-M^2 + \frac{m^2}{\Delta} + \frac{\lambda^2}{1-\Delta})} \; . \end{aligned} \tag{38}$$

Here $r_\perp$ is the magnitude of the transverse momentum of the current quark jet relative to the virtual photon direction, and $\Delta = x_{Bj}$ is the usual Bjorken variable. To obtain (38) from Eq. (21) of [174], we used the correspondence $|e_1 e_2|/4\pi \to C_F \alpha_s(\mu^2)$ and the fact that the sign of the charges e_1 and e_2 of the quark and diquark are opposite since they constitute a bound state. The result can be tested in jet production using an observable such as thrust to define the momentum $q + r$ of the struck quark.

The predictions of our model for the asymmetry $A_{UT}^{\sin\phi}$ of the $\vec{S}_p \cdot \vec{q} \times \vec{p}_q$ correlation based on Eq. (38) are shown in Fig. 15. As representative parameters we take $\alpha_s = 0.3$, $M = 0.94$ GeV for the proton mass, $m = 0.3$ GeV for the fermion constituent and $\lambda = 0.8$ GeV for the spin-0 spectator. The single-spin asymmetry $A_{UT}^{\sin\phi}$ is shown as a function of Δ and $r_\perp$ (GeV). The asymmetry measured at HERMES [223] $A_{UL}^{\sin\phi} = K A_{UT}^{\sin\phi}$ contains a kinematic factor $K = \frac{Q}{\nu}\sqrt{1-y} = \sqrt{\frac{2Mx}{E}}\sqrt{\frac{1-y}{y}}$ because the proton is polarized along the incident electron direction. The resulting prediction for $A_{UL}^{\sin\phi}$ is shown in Fig. 15(b). Note that $\vec{r} = \vec{p}_q - \vec{q}$ is the momentum of the current quark jet relative to the photon momentum. The asymmetry as a function of the pion momentum $\vec{p}_\pi$ requires a convolution with the quark fragmentation function.

Since the same matrix element controls the Pauli form factor, the contribution of each quark current to the SSA is proportional to the contribution $\kappa_{q/p}$ of that quark to the proton target's anomalous magnetic moment $\kappa_p = \sum_q e_q \kappa_{q/p}$ [174, 220]. Avakian [209] has shown that the data from HERMES and Jefferson laboratory could be accounted for by the above analysis. The HERMES collaboration has recently measured the SSA in pion electroproduction using transverse target polarization [224]. The Sivers and Collins effects can be separated using planar correlations; both contributions are observed to contribute, with values not in disagreement with theory expectations.

It should be emphasized that the Sivers effect occurs even for jet production; unlike transversity, hadronization is not required. There is no Sivers effect in charged

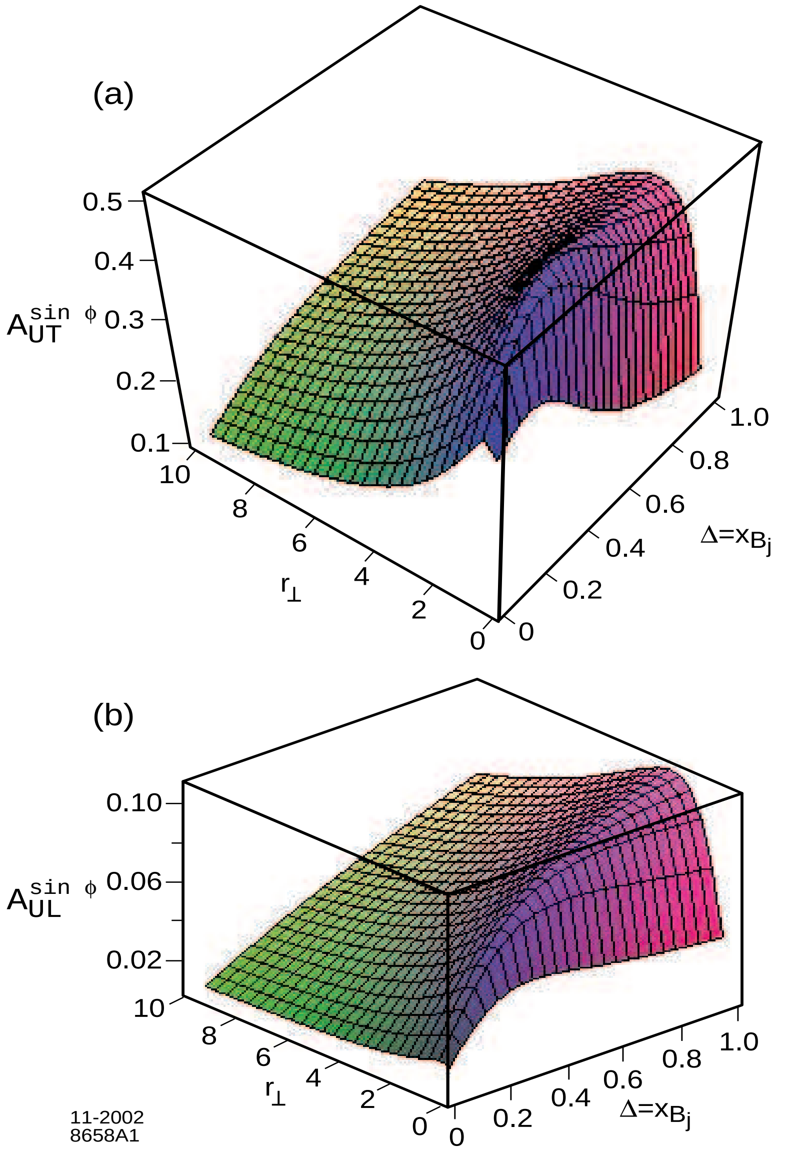

Figure 15: Model predictions for the target single-spin asymmetry $A_{UT}^{\sin\phi}$ for charged and neutral current deep inelastic scattering resulting from gluon exchange in the final state. Here $r_\perp$ is the magnitude of the transverse momentum of the outgoing quark relative to the photon or vector boson direction, and $\Delta = x_{bj}$ is the light-front momentum fraction of the struck quark. The parameters of the model are given in the text. In (a) the target polarization is transverse to the incident lepton direction. The asymmetry in (b) $A_{UL}^{\sin\phi} = K A_{UT}^{\sin\phi}$ includes a kinematic factor $K = \frac{Q}{\nu}\sqrt{1-y}$ for the case where the target nucleon is polarized along the incident lepton direction. For illustration, we have taken $K = 0.26\sqrt{x}$, corresponding to the kinematics of the HERMES experiment [223] with $E_{lab} = 27.6$ GeV and $y = 0.5$.

current reactions since the W only couples to left-handed quarks [225].

The corresponding single spin asymmetry for the Drell-Yan processes, such as $\pi p^{\leftrightarrow}$ (or $pp^{\leftrightarrow}$) $\to \gamma^* X \to \ell^+ \ell^- X$, is due to initial-state interactions. The simplest way to get the result is applying crossing symmetry to the SIDIS processes. The result that the SSA in the Drell-Yan process is the same as that obtained in SIDIS, with the appropriate identification of variables, but with the opposite sign [218, 221].

We can also consider the SSA of e^+e^- annihilation processes such as $e^+e^- \to \gamma^* \to \pi \Lambda^{\leftrightarrow} X$. The Λ reveals its polarization via its decay $\Lambda \to p\pi^-$. The spin of the Λ is normal to the decay plane. Thus we can look for a SSA through the T-odd correlation $\epsilon_{\mu\nu\rho\sigma} S^{\mu}_{\Lambda} p^{\nu}_{\Lambda} q^{\rho}_{\gamma^*} p^{\sigma}_{\pi}$. This is related by crossing to SIDIS on a Λ target.

Measurements from Jefferson Lab [226] also show significant beam single spin asymmetries in deep inelastic scattering. Afanasev and Carlson [227] have recently shown that this asymmetry is due to the interference of longitudinal and transverse photoabsorption amplitudes which have different phases induced by the final-state interaction between the struck quark and the target spectators just as in the calculations of Ref. [174]. Their results are consistent with the experimentally observed magnitude of this effect. Thus similar FSI mechanisms involving quark orbital angular momentum appear to be responsible for both target and beam single-spin asymmetries.

12 New Directions for QCD

As I have emphasized in these lectures, the light-front wavefunctions of hadrons are the central elements of QCD phenomenology, describing bound states in terms of their fundamental quark and gluon degrees of freedom at the amplitude level. Given the light-front wavefunctions one can compute quark and gluon distributions, distribution amplitudes, generalized parton distributions, form factors, and matrix elements of local currents such as semileptonic B decays. The diffractive dissociation of hadrons on nucleons or nuclei into jets or leading hadrons can provide new measures of the LFWFs of the projectile as well as tests of color transparency, hidden color, and intrinsic charm. The advent of the 12 GeV upgrade of the Jefferson Laboratory electron accelerator and the new 15 GeV antiproton storage ring HESR at GSI will open up important new tests of these properties of QCD in hadronic and nuclear reactions.

Although we are still far from solving QCD explicitly, a number of properties of the light-front wavefunctions of the hadrons are known from both phenomenology and the basic properties of QCD. For example, the endpoint behavior of light-front wavefunctions and structure functions can be determined from perturbative arguments and Regge arguments. There are also correspondence principles. For example, for heavy quarks in the nonrelativistic limit, the light-front formalism reduces to conventional many-body Schrödinger theory. On the other hand, one can also build effective three-quark models which encode the static properties of relativistic baryons.

It is thus imperative to compute the light-front wavefunctions from first principles in QCD. Lattice gauge theory can provide moments of the distribution amplitudes by evaluating vacuum-to-hadron matrix elements of local operators [95]. The transverse lattice is also providing new nonperturbative information [93, 94]. The DLCQ method is also a first-principles method for solving nonperturbative QCD; at finite harmonic resolution K the DLCQ Hamiltonian acts in physical Minkowski space as a finite-dimensional Hermitian matrix in Fock space. The DLCQ Heisenberg equation is Lorentz-frame independent and has the advantage of providing not only the spectrum of hadrons, but also the complete set of LFWFs for each hadron eigenstate. An important feature the light-front formalism is that J_z is conserved; thus one simplify the DLCQ method by projecting the full Fock space on states with specific angular momentum. As shown in Ref. [91], the Karmanov-Smirnov operator uniquely specifies the form of the angular dependence of the light-front wavefunctions, allowing one to transform the light-front Hamiltonian equations to differential equations acting on scalar forms. A complementary method would be to construct the T-matrix for asymptotic $q\overline{q}$ or qqq or gluonium states using the light-front analog of the Lippmann-Schwinger method. This allows one to focus on states with the specific global quantum numbers and spin of a given hadron. The zeros of the resulting resolvent then provides the hadron spectrum and the respective light-front Fock state projections.

In principle, the complete spectrum and bound-state wave functions of a quantum field theory can be determined by finding the eigenvalues and eigensolutions of its light-cone Hamiltonian.

The DLCQ method has a number of attractive features for solving 3+1 quantum field theories nonperturbatively because of the ability to truncate the Fock state to low particle number sectors. One of the challenges in obtaining nonperturbative solutions for gauge theories such as QCD using light-cone Hamiltonian methods is to renormalize the theory while preserving Lorentz symmetries and gauge invariance. For example, the truncation of the light-cone Fock space leads to uncompensated ultraviolet divergences. Recently we presented two methods for consistently regularizing light-cone-quantized gauge theories in Feynman and light-cone gauges [228]: (1) the introduction of a spectrum of Pauli-Villars fields which produces a finite theory while preserving Lorentz invariance; (2) the augmentation of the gauge-theory Lagrangian with higher derivatives. Finite-mass Pauli-Villars regulators can also be used to compensate for neglected higher Fock states. As a test case, we have applied these regularization procedures to an approximate nonperturbative computation of the anomalous magnetic moment of the electron in QED as a first attempt to meet Feynman's famous challenge.

12.1 Testing Hidden Color

In traditional nuclear physics, the deuteron is a bound state of a proton and a neutron where the binding force arise from the exchange of a pion and other mesonic states. However, as I have reviewed, QCD provides a new perspective [163, 167].: 6 quarks in the fundamental 3_C representation of $SU(3)$ color can combine into 5 different color-singlet combinations, only one of which corresponds to a proton and neutron In fact, if the deuteron wavefunction is a proton-neutron bound state at large distances, then as their separation becomes smaller, the QCD evolution resulting from colored gluon exchange introduce 4 other "hidden color" states into the deuteron wavefunction [150]. As I have discussed, the normalization of the deuteron form factor observed at large Q^2 [164], as well as the presence of two mass scales in the scaling behavior of the reduced deuteron form factor [163] thus suggests sizable hidden-color Fock state contributions such as $|\,(uud)_{8_C}(ddu)_{8_C}\rangle$ with probability of order 15% in the deuteron wavefunction [165].

The hidden color states of the deuteron can be materialized at the hadron level as $\Delta^{++}(uuu)\Delta^{-}(ddd)$ and other novel quantum fluctuations of the deuteron. These dual hadron components become more and more important as one probes the deuteron at short distances, such as in exclusive reactions at large momentum transfer. For example, the ratio

$$\frac{\frac{d\sigma}{dt}(\gamma d \to \Delta^{++}\Delta^{-})}{\frac{d\sigma}{dt}(\gamma d \to np)}$$

should increase dramatically with increasing transverse momentum p_T. Similarly the Coulomb dissociation of the deuteron into various exclusive channels

$$ed \to e' + pn, pp\pi^{-}, \Delta\Delta, \cdots$$

should have a changing composition as the final-state hadrons are probed at high transverse momentum, reflecting the onset of hidden color degrees of freedom.

12.2 Perspectives on QCD from AdS/CFT

An outstanding consequence of Maldacena's duality [11] between 10-dimensional string theory on $AdS_5 \times S^5$ and conformally invariant Yang-Mills theories [229, 230] is the potential to describe processes for physical QCD which are valid at strong coupling and do not rely on perturbation theory. As shown by Polchinski and Strassler [12], dimensional counting rules [23] for the leading power-law fall-off of hard exclusive scattering can be derived from a gauge theory with a mass gap dual to supergravity in warped spacetimes. The modified theory generates the hard behavior expected from QCD, instead of the soft behavior characteristic of strings. Other examples are the description of form factors at large transverse momentum [231] and deep inelastic scattering [232]. The discussion of scaling laws in warped backgrounds has also been addressed in [233, 13, 14].

The AdS/CFT correspondence has now provided important new information on the short-distance structure of hadronic LFWFs; one obtains conformal constraints which are not dependent on perturbation theory. The large $k_\perp$ fall-off of the valence LFWFs is also rigorously determined by consistency with the evolution equations for the hadron distribution amplitudes [64]. Similarly, one can also use the structure of the evolution equations to constrain the $x \to 1$ endpoint behavior of the LFWFs. One can use these strong constraints on the large $k_\perp$ and $x \to 1$ behavior to model the LFWFs. Such forms can also be used as the initial approximations to the wavefunctions needed for variational methods which minimize the expectation value of the light-front Hamiltonian. The derivation is carried out in terms of the lowest dimensions of interpolating fields near the boundary of AdS, treating the boundary values of the string states $\Psi(x, r)$ as a product of quantized operators which create n-partonic states out of the vacuum [29]. The AdS/CFT derivation validate QCD perturbative results and confirm the dominance of the quark interchange mechanism [234] for exclusive QCD processes at large N_C. The predicted orbital dependence coincides with the fall-off of light-front Fock wavefunctions derived in perturbative QCD [30]. Since all of the Fock states of the LFWF beyond the valence state are a manifestation of quantum fluctuations, it is natural to match quanta to quanta the additional dimensions with the metric fluctuations of the bulk geometry about the fixed AdS background. For example, the quantum numbers of each baryon, including intrinsic spin and orbital angular momentum, are determined by matching the dimensions of the string modes $\Psi(x, r)$, with the lowest dimension of the baryonic interpolating operators in the conformal limit.

The AdS/CFT correspondence also provides a novel way to compute the hadronic spectrum. The essential assumption is to require the hadron wavefunctions to vanish at the fifth-dimensional coordinate $r_0 = \Lambda_{QCD}$. As an example, Fig. 16 shows the orbital spectrum of the nucleon states and in Fig. 17 the Δ orbital resonances recently computed by Guy de Teramond and myself [235]. The values of $\mathcal{M}^2$ are computed as a function of orbital angular momentum L. The nucleon states with intrinsic spin $S = \frac{1}{2}$ lie on a curve below the nucleons with $S = \frac{3}{2}$. We have chosen our boundary conditions by imposing the condition $\Psi^+(x, z_o) = 0$ on the positive chirality modes for $S = \frac{1}{2}$ nucleons, and $\Psi^-_\mu(x, z_o) = 0$ on the chirality minus strings for $S = \frac{3}{2}$. In contrast to the nucleons, all of the know Δ orbital states with $S = \frac{1}{2}$ and $S = \frac{3}{2}$ lie on the same trajectory. The boundary conditions in this case are imposed on the chirality minus string modes. The numerical solution corresponding to the roots of Bessel functions give the nonlinear trajectories indicated in the figures. All the curves correspond to the value $\Lambda_{QCD} = 0.22$ GeV, which is the only actual parameter aside from the choice of the boundary conditions. The results for each trajectory show a clustering of states with the same orbital L, consistent with strongly suppressed spin-orbit forces; this is a severe problem for QCD models using one-gluon exchange. The results also indicate a parity degeneracy between states in the parallel trajectories shown in Fig. 16, as seen by displacing the upper curve by one unit of L to the right.

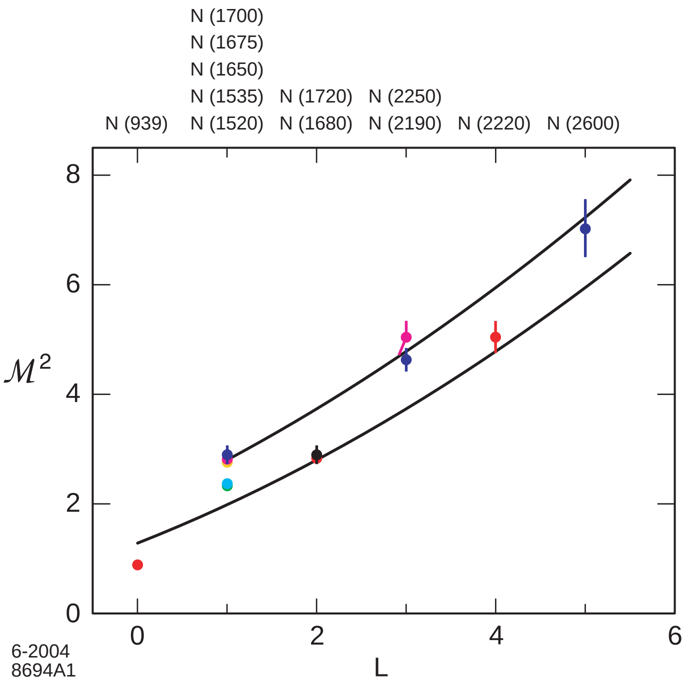

Figure 16: Nucleon orbital spectrum for a value of $\Lambda_{QCD} = 0.22$ GeV. The lower curve corresponds to nucleon states dual to spin-$\frac{1}{2}$ string modes in the bulk. The upper curve corresponds to nucleon states dual to string-$\frac{3}{2}$ modes.

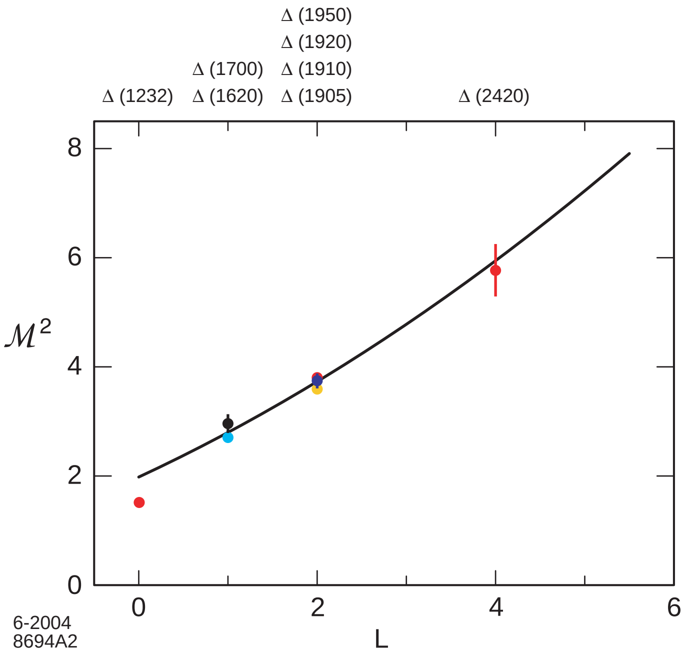

Figure 17: Delta orbital spectrum for $\Lambda_{QCD} = 0.22$ GeV. The Delta states dual to spin-$\frac{1}{2}$ and spin-$\frac{3}{2}$ string modes in the bulk lie on the same trajectory.

Nucleon states with $S = \frac{3}{2}$ and Δ resonances fall on the same trajectory [236].

Since only one parameter, the QCD scale Λ_{QCD}, is used, the agreement of the model with the pattern of the physical light baryon spectrum is remarkable. This agreement possibly reflects the fact that our analysis is based on a conformal template, which is a good initial approximation to QCD [112]. We have chosen a special color representation to construct a three-quark baryon, and the results are effectively independent of N_C. The gauge/string correspondence appears to be a powerful organizing principle to classify and compute the mass eigenvalues of baryon resonances.

Acknowledgments

I wish to thank Guenther Rosner, Stanislav Belostotski, David Ireland, Douglas MacGregor and their colleagues at Glasgow University and Edinburgh University for organizing the 2004 Scottish Universities Summer School in Physics at St. Andrews. These lectures are based on collaborations with Carl Carlson, Guy de Teramond, Markus Diehl, Rikard Enberg, John Hiller, Kent Hornbostel, Paul Hoyer, Dae Sung Hwang, Gunnar Ingelman, Chueng Ji, Volodya Karmanov, Peter Lepage, Gary McCartor, Chris Pauli, Joerg Raufeisen, Johan Rathsman, and Dave Robertson.

References

[1] J. Greensite, Prog. Part. Nucl. Phys. **51**, 1 (2003) [arXiv:hep-lat/0301023].

[2] D. J. Gross and F. Wilczek, Phys. Rev. Lett. **30**, 1343 (1973).

[3] H. D. Politzer, Phys. Rev. Lett. **30**, 1346 (1973).

[4] E. Klempt, arXiv:hep-ex/0101031.

[5] K. Rajagopal and F. Wilczek, arXiv:hep-ph/0011333.

[6] D. H. Rischke, Part. Nucl. Phys. **52**, 197 (2004) [arXiv:nucl-th/0305030].

[7] D. J. Schwarz, Annalen Phys. **12**, 220 (2003) [arXiv:astro-ph/0303574].

[8] J. C. Collins, D. E. Soper and G. Sterman, Adv. Ser. Direct. High Energy Phys. **5**, 1 (1988).

[9] G. T. Bodwin, Phys. Rev. D **31**, 2616 (1985) [Erratum-ibid. D **34**, 3932 (1986)].

[10] S. J. Brodsky and G. P. Lepage, in: *Perturbative Quantum Chromodynamics*, edited by A. H. Mueller (World Scientific, Singapore 1989).

[11] J. M. Maldacena, Adv. Theor. Math. Phys. **2**, 231 (1998) [Int. J. Theor. Phys. **38**, 1113 (1999)] [arXiv:hep-th/9711200].

[12] J. Polchinski and M. J. Strassler, Phys. Rev. Lett. **88**, 031601 (2002) [arXiv:hep-th/0109174].

[13] R. C. Brower and C. I. Tan, Nucl. Phys. B **662**, 393 (2003) [arXiv:hep-th/0207144].

[14] O. Andreev, Phys. Rev. D **67**, 046001 (2003) [arXiv:hep-th/0209256].

[15] H. Fritzsch, M. Gell-Mann and H. Leutwyler, Phys. Lett. B **47**, 365 (1973).

[16] P. A. M. Dirac, Rev. Mod. Phys. **21**, 392 (1949).

[17] S. J. Brodsky, H. C. Pauli and S. S. Pinsky, Phys. Rept. **301**, 299 (1998) [arXiv:hep-ph/9705477].

[18] S. D. Drell and T. M. Yan, Phys. Rev. Lett. **24**, 181 (1970).

[19] S. J. Brodsky and S. D. Drell, Phys. Rev. D **22**, 2236 (1980).

[20] R. L. Jaffe and A. Manohar, Nucl. Phys. B **337**, 509 (1990).

[21] X. D. Ji, Nucl. Phys. Proc. Suppl. **119**, 41 (2003) [arXiv:hep-lat/0211016].

[22] J. Raufeisen and S. J. Brodsky, arXiv:hep-th/0408108.

[23] S. J. Brodsky and G. R. Farrar, Phys. Rev. Lett. **31**, 1153 (1973).

[24] V. A. Matveev, R. M. Muradian and A. N. Tavkhelidze, Lett. Nuovo Cim. **7**, 719 (1973).

[25] S. J. Brodsky and G. R. Farrar, Phys. Rev. D **11**, 1309 (1975).

[26] S. J. Brodsky, Published in *Newport News 2002, Exclusive processes at high momentum transfer 1-33.* [arXiv:hep-ph/0208158.]

[27] S. J. Brodsky, M. Burkardt and I. Schmidt, Nucl. Phys. B **441**, 197 (1995) [arXiv:hep-ph/9401328].

[28] S. J. Rey and J. T. Yee, Eur. Phys. J. C **22**, 379 (2001) [arXiv:hep-th/9803001].

[29] S. J. Brodsky and G. F. de Teramond, Phys. Lett. B **582**, 211 (2004) [arXiv:hep-th/0310227].

[30] X. d. Ji, J. P. Ma and F. Yuan, Phys. Rev. Lett. **90**, 241601 (2003) [arXiv:hep-ph/0301141].

[31] S. J. Brodsky, P. Hoyer, C. Peterson and N. Sakai, Phys. Lett. B **93**, 451 (1980).

[32] S. J. Brodsky and B. Q. Ma, Phys. Lett. B **381**, 317 (1996) [arXiv:hep-ph/9604393].

[33] S. Kretzer, arXiv:hep-ph/0408287.

[34] B. Portheault, arXiv:hep-ph/0406226.

[35] F. Olness *et al.*, arXiv:hep-ph/0312323.

[36] M. Franz, V. Polyakov and K. Goeke, Phys. Rev. D **62**, 074024 (2000) [arXiv:hep-ph/0002240].

[37] S. J. Brodsky, J. C. Collins, S. D. Ellis, J. F. Gunion and A. H. Mueller, DOE/ER/40048-21 P4 *Proc. of 1984 Summer Study on the SSC, Snowmass, CO, Jun 23 - Jul 13, 1984*

[38] B. W. Harris, J. Smith and R. Vogt, Nucl. Phys. B **461**, 181 (1996) [arXiv:hep-ph/9508403].

[39] S. J. Brodsky and M. Karliner, Phys. Rev. Lett. **78**, 4682 (1997) [arXiv:hep-ph/9704379].

[40] S. J. Brodsky and S. Gardner, Phys. Rev. D **65**, 054016 (2002) [arXiv:hep-ph/0108121].

[41] C. T. Munger, S. J. Brodsky and I. Schmidt, Phys. Rev. D **49**, 3228 (1994).

[42] F. Halzen, arXiv:astro-ph/0402083.

[43] P. Hoyer, M. Vanttinen and U. Sukhatme, Phys. Lett. B **246**, 217 (1990).

[44] J. Badier *et al.* [NA3 Collaboration], Phys. Lett. B **104**, 335 (1981).

[45] J. C. Anjos, J. Magnin and G. Herrera, Phys. Lett. B **523**, 29 (2001) [arXiv:hep-ph/0109185].

[46] A. Ocherashvili *et al.* [SELEX Collaboration], arXiv:hep-ex/0406033.

[47] S. J. Brodsky, A. S. Goldhaber, and M. Karliner, in progress.

[48] R. Vogt and S. J. Brodsky, Phys. Lett. B **349**, 569 (1995) [arXiv:hep-ph/9503206].

[49] B. Andersson, G. Gustafson, G. Ingelman and T. Sjostrand, Phys. Rept. **97**, 31 (1983).

[50] G. Bari *et al.*, Nuovo Cim. A **104**, 1787 (1991).

[51] G. Bertsch, S. J. Brodsky, A. S. Goldhaber and J. F. Gunion, Phys. Rev. Lett. **47**, 297 (1981).

[52] S. J. Brodsky and A. H. Mueller, Phys. Lett. B **206**, 685 (1988).

[53] D. Ashery, Comments Nucl. Part. Phys. **2**, A235 (2002).

[54] A. B. Borisov [HERMES Collaboration], Nucl. Phys. A **711**, 269 (2002).

[55] J. Aclander *et al.*, arXiv:nucl-ex/0405025.

[56] S. J. Brodsky and G. F. de Teramond, Phys. Rev. Lett. **60**, 1924 (1988).

[57] L. Frankfurt, G. A. Miller and M. Strikman, Found. Phys. **30**, 533 (2000) [arXiv:hep-ph/9907214].

[58] N. N. Nikolaev, W. Schafer and G. Schwiete, Phys. Rev. D **63**, 014020 (2001) [arXiv:hep-ph/0009038].

[59] E. M. Aitala *et al.* [E791 Collaboration], Phys. Rev. Lett. **86**, 4773 (2001) [arXiv:hep-ex/0010044].

[60] E. M. Aitala *et al.* [E791 Collaboration], Phys. Rev. Lett. **86**, 4768 (2001) [arXiv:hep-ex/0010043].

[61] J. Gronberg *et al.* [CLEO Collaboration], Phys. Rev. D **57**, 33 (1998) [arXiv:hep-ex/9707031].

[62] G. P. Lepage and S. J. Brodsky, Phys. Lett. B **87**, 359 (1979).

[63] A. V. Efremov and A. V. Radyushkin, Theor. Math. Phys. **42**, 97 (1980) [Teor. Mat. Fiz. **42**, 147 (1980)].

[64] G. P. Lepage and S. J. Brodsky, Phys. Rev. D **22**, 2157 (1980).

[65] H. C. Pauli and S. J. Brodsky, Phys. Rev. D **32**, 1993 (1985).

[66] G. 't Hooft, Nucl. Phys. B **75**, 461 (1974).

[67] K. Hornbostel, S. J. Brodsky and H. C. Pauli, Phys. Rev. D **41**, 3814 (1990).

[68] M. Burkardt, Nucl. Phys. A **504**, 762 (1989).

[69] H. C. Pauli and S. J. Brodsky, Phys. Rev. D **32**, 2001 (1985).

[70] T. Eller, H. C. Pauli and S. J. Brodsky, Phys. Rev. D **35**, 1493 (1987).

[71] G. McCartor, Z. Phys. C **52**, 611 (1991).

[72] G. McCartor, Z. Phys. C **64**, 349 (1994) [arXiv:hep-th/9406094].

[73] A. Harindranath and J. P. Vary, Phys. Rev. D **36**, 1141 (1987).

[74] A. Harindranath and J. P. Vary, Phys. Rev. D **37**, 3010 (1988).

[75] M. Burkardt, Nucl. Phys. A **504**, 762 (1989).

[76] K. Demeterfi, I. R. Klebanov and G. Bhanot, Nucl. Phys. B **418**, 15 (1994) [arXiv:hep-th/9311015].

[77] S. Dalley and I. R. Klebanov, Phys. Rev. D **47**, 2517 (1993) [arXiv:hep-th/9209049].

[78] M. Burkardt, Phys. Rev. D **47**, 4628 (1993).

[79] M. Krautgartner, H. C. Pauli and F. Wolz, Phys. Rev. D **45**, 3755 (1992). PHRVA,D45,3755;

[80] M. Kaluza and H. C. Pauli, Phys. Rev. D **45**, 2968 (1992).

[81] S. J. Brodsky, J. R. Hiller and G. McCartor, Annals Phys. **305**, 266 (2003) [arXiv:hep-th/0209028].

[82] C. J. Hamer, Nucl. Phys. B **195**, 503 (1982).

[83] G. D. Date, Y. Frishman and J. Sonnenschein, Nucl. Phys. B **283**, 365 (1987).

[84] S. J. Brodsky and D. S. Hwang, Nucl. Phys. B **543**, 239 (1999) [arXiv:hep-ph/9806358].

[85] S. J. Brodsky, D. S. Hwang, B. Q. Ma and I. Schmidt, Nucl. Phys. B **593**, 311 (2001) [arXiv:hep-th/0003082].

[86] S. J. Brodsky, M. Diehl and D. S. Hwang, Nucl. Phys. B **596**, 99 (2001) [arXiv:hep-ph/0009254].

[87] S. J. Brodsky, P. Hoyer, N. Marchal, S. Peigne and F. Sannino, Phys. Rev. D **65**, 114025 (2002) [arXiv:hep-ph/0104291].

[88] F. Antonuccio, S. J. Brodsky and S. Dalley, Phys. Lett. B **412**, 104 (1997) [arXiv:hep-ph/9705413].

[89] V. A. Karmanov and A.V. Smirnov, Nucl. Phys. A **546**, 691 (1992).

[90] J. Carbonell, B. Desplanques, V. A. Karmanov, and J. F. Mathiot, Phys. Rep. **300**, 215 (1998) [arXiv:nucl-th/9804029].

[91] S. J. Brodsky, J. R. Hiller, D. S. Hwang and V. A. Karmanov, Phys. Rev. D **69**, 076001 (2004) [arXiv:hep-ph/0311218].

[92] W. A. Bardeen, R. B. Pearson and E. Rabinovici, Phys. Rev. D **21**, 1037 (1980).

[93] S. Dalley, arXiv:hep-ph/0409139.

[94] M. Burkardt and S. Dalley, Prog. Part. Nucl. Phys. **48**, 317 (2002) [arXiv:hep-ph/0112007].

[95] L. Del Debbio, M. Di Pierro, A. Dougall and C. T. Sachrajda [UKQCD collaboration], Nucl. Phys. Proc. Suppl. **83**, 235 (2000) [arXiv:hep-lat/9909147].

[96] P. Maris and C. D. Roberts, Int. J. Mod. Phys. E **12**, 297 (2003) [arXiv:nucl-th/0301049].

[97] D. J. Gross, A. Hashimoto and I. R. Klebanov, Phys. Rev. D **57**, 6420 (1998) [arXiv:hep-th/9710240].

[98] M. Harada, J. R. Hiller, S. Pinsky and N. Salwen, Phys. Rev. D **70**, 045015 (2004) [arXiv:hep-th/0404123].

[99] M. van Iersel and B. L. G. Bakker, arXiv:hep-ph/0407318. B. L. G. Bakker, M. van Iersel, and F. Pijlman, Few-Body Systems **33**, 27 (2003).

[100] H. C. Pauli, arXiv:hep-ph/0312300.

[101] M. Weinstein, arXiv:hep-th/0410113.

[102] H. Zhan, A. Nogga, B. R. Barrett, J. P. Vary and P. Navratil, Phys. Rev. C **69**, 034302 (2004) [arXiv:nucl-th/0401047].

[103] S. Dalley, Nucl. Phys. B (Proc. Suppl.) **108**, 145 (2002).

[104] S. J. Brodsky, Published in *Nagoya 2002, Strong coupling gauge theories and effective field theories, 1-18.* [arXiv:hep-th/0304106].

[105] K. G. Wilson, Phys. Rept. **23**, 331 (1976).

[106] T. DeGrand, Int. J. Mod. Phys. A **19**, 1337 (2004) [arXiv:hep-ph/0312241].

[107] G. Parisi, Phys. Lett. B **39**, 643 (1972).

[108] S. J. Brodsky, E. Gardi, G. Grunberg and J. Rathsman, Phys. Rev. D **63**, 094017 (2001) [arXiv:hep-ph/0002065].

[109] J. Rathsman, in *Proc. of the 5th International Symposium on Radiative Corrections (RADCOR 2000)* ed. Howard E. Haber, arXiv:hep-ph/0101248.

[110] G. Grunberg, JHEP **0108**, 019 (2001) [arXiv:hep-ph/0104098].

[111] T. Banks and A. Zaks, Nucl. Phys. B **196**, 189 (1982).

[112] S. J. Brodsky, arXiv:hep-ph/0408069.

[113] S. J. Brodsky, SLAC-PUB-10206 *Invited talk at International Conference on Color Confinement and Hadrons in Quantum Chromodynamics - Confinement 2003, Wako, Japan, 21-24 Jul 2003*

[114] S. J. Brodsky, Y. Frishman, G. P. Lepage and C. Sachrajda, Phys. Lett. **91B**, 239 (1980).

[115] S. J. Brodsky, P. Damgaard, Y. Frishman and G. P. Lepage, Phys. Rev. D **33**, 1881 (1986).

[116] S. J. Brodsky, Y. Frishman and G. P. Lepage, Phys. Lett. B **167**, 347 (1986).

[117] V. M. Braun, G. P. Korchemsky and D. Muller, Prog. Part. Nucl. Phys. **51**, 311 (2003) [arXiv:hep-ph/0306057].

[118] S. J. Brodsky and G. P. Lepage, SLAC-PUB-4947 *In *A.H. Mueller, (ed): Perturbative Quantum Chromodynamics, 1989, p. 93-240,* and S. J. Brodsky, SLAC-PUB-8649 *In *Shifman, M. (ed.): At the frontier of particle physics, Handbook of QCD: Boris Ioffe Festschrift, vol. 2*, 2001, p 1343-1444.*

[119] S. J. Brodsky and H. J. Lu, Phys. Rev. D **51**, 3652 (1995) [arXiv:hep-ph/9405218].

[120] S. J. Brodsky, G. P. Lepage and P. B. Mackenzie, Phys. Rev. D **28**, 228 (1983).

[121] S. J. Brodsky, G. T. Gabadadze, A. L. Kataev and H. J. Lu, Phys. Lett. **B372**, 133 (1996) [arXiv:hep-ph/9512367].

[122] R. J. Crewther, Phys. Rev. Lett. **28**, 1421 (1972).

[123] S. J. Brodsky, C. R. Ji, A. Pang and D. G. Robertson, Phys. Rev. D **57**, 245 (1998) [arXiv:hep-ph/9705221].

[124] J. M. Cornwall, Phys. Rev. D **26**, 1453 (1982).

[125] L. von Smekal, R. Alkofer and A. Hauck, Phys. Rev. Lett. **79**, 3591 (1997) [arXiv:hep-ph/9705242].

[126] D. Zwanziger, Phys. Rev. D **69**, 016002 (2004) [arXiv:hep-ph/0303028].

[127] D. M. Howe and C. J. Maxwell, Phys. Lett. B **541**, 129 (2002) [arXiv:hep-ph/0204036].

[128] D. M. Howe and C. J. Maxwell, Phys. Rev. D **70**, 014002 (2004) [arXiv:hep-ph/0303163].

[129] S. Furui and H. Nakajima, arXiv:hep-lat/0309166.

[130] S. Furui and H. Nakajima, arXiv:hep-lat/0403021.

[131] A. M. Badalian and A. I. Veselov, arXiv:hep-ph/0407082.

[132] K. Ackerstaff *et al.* [OPAL Collaboration], Eur. Phys. J. C **7**, 571 (1999) [arXiv:hep-ex/9808019].

[133] A. C. Mattingly and P. M. Stevenson, Phys. Rev. D **49**, 437 (1994) [arXiv:hep-ph/9307266].

[134] S. J. Brodsky, S. Menke, C. Merino and J. Rathsman, Phys. Rev. D **67**, 055008 (2003) [arXiv:hep-ph/0212078].

[135] M. Baldicchi and G. M. Prosperi, Phys. Rev. D **66**, 074008 (2002) [arXiv:hep-ph/0202172].

[136] F. Le Diberder and A. Pich, *Phys. Lett.* **B289**, 165 (1992).

[137] M. Beneke and V. M. Braun, *Phys. Lett.* **B348**, 513 (1995) [arXiv:hep-ph/9411229].

[138] P. Ball, M. Beneke and V. M. Braun, *Nucl. Phys.* **B452**, 563 (1995) [arXiv:hep-ph/9502300].

[139] Y. L. Dokshitzer, G. Marchesini and B. R. Webber, *Nucl. Phys.* **B469**, 93 (1996) [arXiv:hep-ph/9512336].

[140] B. Melic, B. Nizic and K. Passek, Phys. Rev. D **65**, 053020 (2002) [arXiv:hep-ph/0107295].

[141] S. J. Brodsky and P. Huet, Phys. Lett. B **417**, 145 (1998) [arXiv:hep-ph/9707543].

[142] P. V. Landshoff, Phys. Rev. D **10**, 1024 (1974).

[143] S. J. Brodsky and G. P. Lepage, SLAC-PUB-2294 *Workshop on Current Topics in High Energy Physics*, Cal Tech., Pasadena, Calif., Feb 13-17, 1979.

[144] G. P. Lepage and S. J. Brodsky, Phys. Rev. Lett. **43**, 545 (1979).

[145] A. V. Efremov and A. V. Radyushkin, Theor. Math. Phys. **42** (1980) 97;

[146] D. Muller, Phys. Rev. D **51**, 3855 (1995) [arXiv:hep-ph/9411338].

[147] P. Ball and V. M. Braun, Nucl. Phys. B **543**, 201 (1999) [arXiv:hep-ph/9810475].

[148] V. M. Braun, S. E. Derkachov, G. P. Korchemsky and A. N. Manashov, Nucl. Phys. **B553**, 355 (1999) [arXiv:hep-ph/9902375].

[149] S. J. Brodsky and G. P. Lepage, Phys. Rev. D **24**, 2848 (1981).

[150] S. J. Brodsky, C. R. Ji and G. P. Lepage, Phys. Rev. Lett. **51**, 83 (1983).

[151] S. J. Brodsky and G. P. Lepage, Phys. Rev. D **24**, 1808 (1981).

[152] For a review of QCD tests in photon-photon collisions see, S. J. Brodsky, in *Proc. of the* e^+e^- *Physics at Intermediate Energies Conference* ed. Diego Bettoni, eConf **C010430**, W01 (2001) [arXiv:hep-ph/0106294].

[153] M. Beneke, G. Buchalla, M. Neubert and C. T. Sachrajda, Nucl. Phys. B **591**, 313 (2000) [arXiv:hep-ph/0006124].

[154] Y. Y. Keum, H. N. Li and A. I. Sanda, Phys. Rev. D **63**, 054008 (2001) [arXiv:hep-ph/0004173].

[155] A. Szczepaniak, E. M. Henley and S. J. Brodsky, Phys. Lett. B **243**, 287 (1990).

[156] A review of QCD analyses of exclusive B decays is given in S. J. Brodsky, Published in *Ise-Shima 2001, B physics and CP violation, 229-234* [arXiv:hep-ph/0104153].

[157] C. K. Chua, W. S. Hou and S. Y. Tsai, Phys. Rev. D **66**, 054004 (2002) [arXiv:hep-ph/0204185].

[158] R. J. Holt, Phys. Rev. **C41**, 2400 (1990).

[159] C. Bochna *et al.* [E89-012 Collaboration], Phys. Rev. Lett. **81**, 4576 (1998) [arXiv:nucl-ex/9808001].

[160] P. Rossi *et al.* [CLAS Collaboration], arXiv:hep-ph/0405207.

[161] A. Duncan and A. H. Mueller, Phys. Rev. D **21**, 1636 (1980). See also S. J. Brodsky, Y. Frishman, G. P. Lepage, and C. Sachrajda, Phys. Lett. 91B, 239 (1980). A. Duncan and A. H. Mueller, Phys. Rev. D 21, 1636 (1080). M. Peskin, Phys. Lett. 88B, 128 (1979). A. V. Efremov and A. V. Radyushkin, Phys. Lett. 04B, 245 (1980).

[162] S. J. Brodsky and B. T. Chertok, Phys. Rev. Lett. **37**, 269 (1976).

[163] S. J. Brodsky and B. T. Chertok, Phys. Rev. D **14**, 3003 (1976).

[164] R. G. Arnold *et al.*, Phys. Rev. Lett. **35**, 776 (1975).

[165] G. R. Farrar, K. Huleihel and H. y. Zhang, Phys. Rev. Lett. **74**, 650 (1995).

[166] M. Harvey, Nucl. Phys. A **352**, 326 (1981).

[167] V. A. Matveev and P. Sorba, Lett. Nuovo Cim. **20**, 435 (1977).

[168] A. V. Belitsky, X. D. Ji and F. Yuan, Phys. Rev. Lett. **91**, 092003 (2003) [arXiv:hep-ph/0212351].

[169] M. K. Jones *et al.* [Jefferson Lab Hall A Collaboration], Phys. Rev. Lett. **84**, 1398 (2000) [arXiv:nucl-ex/9910005].

[170] Y. C. Chen, A. Afanasev, S. J. Brodsky, C. E. Carlson and M. Vanderhaeghen, arXiv:hep-ph/0403058.

[171] S. J. Brodsky, C. E. Carlson, J. R. Hiller and D. S. Hwang, Phys. Rev. D **69**, 054022 (2004) [arXiv:hep-ph/0310277].

[172] J. D. Bjorken, Phys. Rev. **179**, 1547 (1969).

[173] E. D. Bloom *et al.*, Phys. Rev. Lett. **23**, 930 (1969).

[174] S. J. Brodsky, D. S. Hwang and I. Schmidt, Phys. Lett. B **530**, 99 (2002) [arXiv:hep-ph/0201296].

[175] S. J. Brodsky and H. J. Lu, Phys. Rev. Lett. **64**, 1342 (1990).

[176] S. J. Brodsky, R. Enberg, P. Hoyer and G. Ingelman, arXiv:hep-ph/0409119.

[177] A. V. Belitsky, X. Ji and F. Yuan, Nucl. Phys. B **656**, 165 (2003) [arXiv:hep-ph/0208038].

[178] J. C. Collins and A. Metz, arXiv:hep-ph/0408249.

[179] J. C. Collins, Phys. Lett. B **536**, 43 (2002) [arXiv:hep-ph/0204004].

[180] J. C. Collins, arXiv:hep-ph/0304122.

[181] D. W. Sivers, Phys. Rev. D **43**, 261 (1991).

[182] S. J. Brodsky, I. Schmidt and J. J. Yang, arXiv:hep-ph/0409279.

[183] G. P. Zeller *et al.* [NuTeV Collaboration], Phys. Rev. Lett. **88**, 091802 (2002) [Erratum-ibid. **90**, 239902 (2003)] [arXiv:hep-ex/0110059].

[184] H. Abramowicz, in *Proc. of the 19th Intl. Symp. on Photon and Lepton Interactions at High Energy LP99* ed. J.A. Jaros and M.E. Peskin, Int. J. Mod. Phys. A **15S1**, 495 (2000) [eConf **C990809**, 495 (2000)] [arXiv:hep-ph/0001054].

[185] C. Adloff *et al.* [H1 Collaboration], Z. Phys. C **76**, 613 (1997) [arXiv:hep-ex/9708016].

[186] J. Breitweg *et al.* [ZEUS Collaboration], Eur. Phys. J. C **6**, 43 (1999) [arXiv:hep-ex/9807010].

[187] J. Raufeisen, arXiv:hep-ph/0009358.

[188] S. J. Brodsky, L. Frankfurt, J. F. Gunion, A. H. Mueller and M. Strikman, Phys. Rev. D **50**, 3134 (1994) [arXiv:hep-ph/9402283].

[189] R. J. Glauber, Phys. Rev. **100**, 242 (1955).

[190] V. N. Gribov, Sov. Phys. JETP **30**, 709 (1970) [Zh. Eksp. Teor. Fiz. **57**, 1306 (1969)].

[191] V. N. Gribov, Sov. Phys. JETP **29**, 483 (1969) [Zh. Eksp. Teor. Fiz. **56**, 892 (1969)].

[192] L. Stodolsky, Phys. Rev. Lett. **18**, 135 (1967).

[193] S. J. Brodsky and J. Pumplin, Phys. Rev. **182** (1969) 1794.

[194] S. J. Brodsky and H. J. Lu, Phys. Rev. Lett. **64** (1990) 1342.

[195] B. L. Ioffe, Phys. Lett. B **30**, 123 (1969).

[196] L. L. Frankfurt and M. I. Strikman, Nucl. Phys. B **316**, 340 (1989).

[197] B. Z. Kopeliovich, J. Raufeisen and A. V. Tarasov, Phys. Lett. B **440**, 151 (1998) [arXiv: hep-ph/9807211].

[198] D. E. Kharzeev and J. Raufeisen, nucl-th/0206073, and references therein.

[199] A. H. Mueller and A. I. Shoshi, arXiv:hep-ph/0402193.

[200] J. w. Qiu and I. Vitev, arXiv:hep-ph/0405068.

[201] A. D. Martin, M. G. Ryskin and G. Watt, arXiv:hep-ph/0406224.

[202] M. Ruspa, Acta Phys. Polon. B **35**, 473 (2004).

[203] J. Kuti and V. F. Weisskopf, Phys. Rev. D **4**, 3418 (1971).

[204] M. Arneodo, Phys. Rept. **240**, 301 (1994).

[205] S. J. Brodsky, I. Schmidt and J. J. Yang, arXiv:hep-ph/0409279.

[206] K. S. McFarland *et al.*, Int. J. Mod. Phys. A **18**, 3841 (2003).

[207] R. Petti, (NOMAD collaboration) presented at ICHEP(2004).

[208] Steve Geer, hep-ph/0210113, Talk given at 4th NuFact '02 Workshop (Neutrino Factories based on Muon Storage Rings), London, England, 1-6 Jul 2002.

[209] H. Avakian [CLAS Collaboration], *Workshop on Testing QCD through Spin Observables in Nuclear Targets, Charlottesville, Virginia, 18-20 Apr 2002*

[210] R.L. Jaffe, hep-ph/9602236.

[211] D. Boer, Nucl. Phys. Proc. Suppl. **105**, 76 (2002) [hep-ph/0109221].

[212] D. Boer, Nucl. Phys. **A 711**, 21 (2002) [hep-ph/0206235].

[213] J.C. Collins, Nucl. Phys. **B 396**, 161 (1993).

[214] V. Barone, A. Drago and P.G. Ratcliffe, Phys. Rept. **359**, 1 (2002).

[215] B. Q. Ma, I. Schmidt and J. J. Yang, Phys. Rev. D **66**, 094001 (2002) [arXiv:hep-ph/0209114].

[216] G. R. Goldstein and L. Gamberg, arXiv:hep-ph/0209085.

[217] L. P. Gamberg, G. R. Goldstein and K. A. Oganessyan, Phys. Rev. D **67**, 071504 (2003) [arXiv:hep-ph/0301018].

[218] J.C. Collins, Phys. Lett. **B 536**, 43 (2002).

[219] X. Ji and F. Yuan, Phys. Lett. **B 543**, 66 (2002).

[220] M. Burkardt, arXiv:hep-ph/0408009.

[221] S.J. Brodsky, D.S. Hwang and I. Schmidt, Nucl. Phys. **B 642**, 344 (2002).

[222] D. Boer, S. J. Brodsky and D. S. Hwang, Phys. Rev. D **67**, 054003 (2003) [arXiv:hep-ph/0211110].

[223] A. Airapetian *et al.* [HERMES Collaboration], Phys. Rev. Lett. **84**, 4047 (2000).

[224] A. Airapetian *et al.* [HERMES Collaboration], arXiv:hep-ex/0408013.

[225] S. J. Brodsky, D. S. Hwang and I. Schmidt, Phys. Lett. B **553**, 223 (2003) [arXiv:hep-ph/0211212].

[226] H. Avakian *et al.* [CLAS Collaboration], arXiv:hep-ex/0301005.

[227] A. Afanasev and C. E. Carlson, arXiv:hep-ph/0308163.

[228] S. J. Brodsky, V. A. Franke, J. R. Hiller, G. McCartor, S. A. Paston and E. V. Prokhvatilov, arXiv:hep-ph/0406325.

[229] S. S. Gubser, I. R. Klebanov and A. M. Polyakov, Phys. Lett. B **428**, 105 (1998) [arXiv:hep-th/9802109].

[230] E. Witten, Adv. Theor. Math. Phys. **2**, 253 (1998) [arXiv:hep-th/9802150].

[231] J. Polchinski and L. Susskind, arXiv:hep-th/0112204.

[232] J. Polchinski and M. J. Strassler, JHEP **0305**, 012 (2003) [arXiv:hep-th/0209211].

[233] H. Boschi-Filho and N. R. Braga, Phys. Lett. B **560**, 232 (2003) [arXiv:hep-th/0207071]; arXiv:hep-th/0312231.

[234] J. F. Gunion, S. J. Brodsky and R. Blankenbecler, Phys. Lett. B **39**, 649 (1972); Phys. Rev. **D8**, 287 (1973).

[235] G. F. de Teramond and S. J. Brodsky, arXiv:hep-th/0409074.

[236] E. Klempt, arXiv:hep-ph/0404270.